

Bayesian inference and non-linear extensions of the CIRCE method for quantifying the uncertainty of closure relationships integrated into thermal-hydraulic system codes

Guillaume Damblin^{a,*}, Pierre Gaillard^{a,1}

^a*CEA Saclay - DEN/DANS/DM2S/STMF - F-91191 Gif-sur-Yvette Cedex, France*

Abstract

Uncertainty Quantification of closure relationships integrated into thermal-hydraulic system codes is a critical prerequisite so that the Best-Estimate Plus Uncertainty (BEPU) methodology for nuclear safety and licensing processes can be implemented. This issue has been subject to several international initiatives, such as BEMUSE and PREMIUM projects, as well as statistical developments of which the so-called “CIRCE” method belongs to. The CIRCE method has been developed at the end of the twentieth century, then extensively used for quantifying the uncertainty of closure relationships integrated into the thermal-hydraulic system code CATHARE.

The goal of the CIRCE method is to estimate the (log)-Gaussian probability distribution of a multiplicative factor applied to a reference closure relationship in order to assess its uncertainty. Although this method has been applied with success in numerous physical scenarios, its implementation can still suffer from substantial limitations such as the linearity assumption and the failure to take into account the inherent statistical uncertainty. In the paper, we propose to extend the CIRCE method in two aspects. On the one hand, we adopt the Bayesian setting which puts prior probability distributions on the parameters of the (log)-Gaussian distribution. The posterior distribution of these parameters is then computed with respect to an experimental database by means of Monte Carlo Markov Chain (MCMC) algorithms. On the other hand, we tackle the more general setting where the simulations do not move linearly against the values taken by the multiplicative factor(s). However, MCMC algorithms become time-prohibitive once thermal-hydraulic simulations exceed a few minutes. The method that we have implemented to overcome this handicap relies on the use of a Gaussian process (GP) emulator which can yield both reliable and fast predictions of the simulations.

In the second part of the paper, the MCMC algorithms will be applied to quantify the uncertainty of two condensation models at the safety injections with respect to a database of experimental tests. The thermal-hydraulic simulations will be run with the CATHARE 2 computer code.

*Corresponding author

Email addresses: guillaume.damblin@cea.fr (Guillaume Damblin), pierre.gaillard@framatome.com (Pierre Gaillard)

¹The main content of the paper was done when Pierre Gaillard worked in CEA. He is currently working in Framatome. Present address: Framatome - 1, place de la Coupole - Jean-Millier - 92400 Courbevoie, France

1. Introduction

The use of Best-Estimate system codes for nuclear applications in line with the so-called BEPU (Best-estimate Plus Uncertainty) methodology has been encouraged from several years for reactor transient simulations and safety analysis. This includes code development as well as V&V (Verification and Validation) and UQ (Uncertainty Quantification) efforts. The paper written by D’Auria et al. (2012) gives an overview of the best practices to be applied for safety demonstration in the nuclear community and how the BEPU approach is able to achieve them. As its name implies, the second stage of any BEPU methodology aims to quantify uncertainties related to the numerical simulation of the thermal-hydraulic transient. These can have multiple origins but it is commonly admitted that we can split them into two categories: those of numerical nature (out of the scope of the paper), and those related to the modeling of the physical phenomena. The Verification step aims to assess the formers, essentially by fixing code bugs and computing discretization errors induced by mesh size. Then, the Validation step aims to quantify the inherent gap between the simulations and the real system by means of some carefully chosen physical experiments used as references (Barrayri et al., 2007). In the last two decades, the research dedicated to V&V and UQ activities has been fruitful, leading to the development of exhaustive guidelines in various fields from computational fluid dynamics (AIAA, 1998) to mechanics (ASME, 2009). Those standards provide general V&V and UQ requirements which help improving the methods originally implemented by thermal-hydraulic engineers (Unal et al., 2011) such as CSAU (Boyack et al., 1990) and GRS method (Glaeser, 2008). These methods have been developed by the US Nuclear Regulatory Commission (NRC) and the German nuclear safety institution respectively. Both of them are forward methods where the uncertainties are propagated through the code from the inputs to the outputs of interest. Their implementation for accidental transients at the full reactor scale has been the subject of the BEMUSE² program (De Crécy et al., 2008). The scope of this program was to perform LB-LOCA³ analyses in order to check whether both scaling and uncertainty propagation were able to perform sufficiently well. The probability distributions of uncertain input parameters were known in BEMUSE because their determination was not the aim of the analysis. This issue has been actually studied in two further international projects called PREMIUM⁴ (Csni, 2016), following by the on-going project SAPIUM⁵ (Baccou et al., 2018). The former aimed to compare in a reflood scenario the performance of several methodologies for quantifying the uncertainty of closure relationships, including, in particular, the one of CEA called CIRCE⁶. and the Fast Fourier Transform-based method (Freixa et al., 2016). Unfortunately, the lack of consensus as well as the various practices between the participants raised the need of establishing guidelines and providing general recommendations on how this issue should be addressed. This is the goal of the SAPIUM project.

One of the main source of uncertainty is the one that affects the physical models used as closure relationships in thermal-hydraulic system codes. Such codes rely on a two phase flow six equations model, consisting of three balance equations for the liquid phase and three for the

²Best Estimate Methods Uncertainty and Sensitivity Evaluation

³Large Break - Loss Of Coolant Accident

⁴Post-BEMUSE REflood Models Input Uncertainty Methods

⁵Systematic Approach for Input Uncertainty Quantification

⁶In French the acronym “CIRCE” means *Calcul des Incertitudes Relatives aux Corrélations Élémentaires*

steam phase (mass, momentum and energy for each phase). The solution of such equations depends on closure relationships constructed from appropriate physical experiments called SETs (Separate Effect Tests). The SETs, often performed at a reduced scale compared to that of actual reactors, are instrumented in order to focus on some experimental Quantities of Interest (QoIs) as independently as possible of potential interactions with other phenomena. Based on a careful analysis of such tests, the closure relationships can then be established by thermal-hydraulic engineers. At the end of this process, however, a model-form uncertainty still remains due to both the lack of complete knowledge in the mathematical formulation of the closure relationship and the experimental uncertainty. The former source of uncertainty is often dominant and arises from lack of knowledge, also called epistemic uncertainty. The CIRCE method, introduced by (De Crécy and Bazin, 2001), promotes a probabilistic treatment of such uncertainty where a random multiplicative factor is applied to every reference model. An extra assumption is to model such a factor as either a Gaussian or log-Gaussian probability distribution whose parameters are then estimated from the differences between the experimental QoIs and the corresponding simulations run with the code.

In the paper, the Bayesian framework is deployed instead of Maximum Likelihood Estimation. This is an effective way to take into account the statistical uncertainty through the specification of random variables on the uncertain parameters. Furthermore, we lay out an extension of the CIRCE method where the code outputs do not move linearly against the values of the multiplicative factor(s).

Section 2 lays out the foundations of the CIRCE method, and the statistical equation linked to it. Section 3 deals with MCMC⁷ sampling for Bayesian estimation in the linear setting. Section 4 goes ahead with the non linear setting and explains how it modifies MCMC sampling. In Section 5, we apply these MCMC algorithms to the COSI (Condensation at the Safety Injection) test facilities in order to assess the uncertainty of two condensation models at a safety injection. In Section 6, we end by providing conclusions as well as discussions for future works.

2. The CIRCE method

2.1. Motivation

The CIRCE method is devoted to Uncertainty Quantification (UQ) of physical models integrated into thermal-hydraulic system codes. Such models play the role of closure relationships within the conservation equations on which the code is based. In a BEPU context, the implementation of the CIRCE method is motivated by the requirement of assessing the uncertainty of the critical nuclear quantities being simulated, such as the peak cladding temperature (PCT). This can be done by propagating through the code the uncertainty of the physical models to the PCT (if possible, both scaling and systematic biases should be taken into account as well).

Prior to such forward UQ stage, physical models are established by nuclear engineers from one or several experimental database(s). The reference formulation of a physical model is written in the paper as

$$M_{ref}(\mathbf{x}) \tag{1}$$

⁷Markov Chain Monte Carlo

with \mathbf{x} being a vector including thermal-hydraulic conditions such as pressure, temperature, geometrical properties, dimensionless numbers, void fraction, and so on. As such reference models are tainted by some degree of empiricism in their mathematical forms, quantifying their uncertainties is compulsory before a BEPU approach is implemented. For this purpose, the CIRCE method applies a multiplicative factor λ to every reference model of the code. This assumption allows to measure a relative uncertainty, which is suited to deal with databases having different orders of magnitude. Hence, a thermal-hydraulic simulation can be run with respect to a perturbed model $M_\lambda(\mathbf{x})$ where

$$M_\lambda(\mathbf{x}) = \lambda \times M_{ref}(\mathbf{x}). \quad (2)$$

The more the value of λ moves away from $\lambda = 1$, the more the engineer should question the accuracy of the reference model. In various physical contexts, plausible bounds can be specified around $\lambda = 1$ using expert knowledge. Yet, it remains unclear how to measure the uncertainty between the lower and the upper bound. The CIRCE method actually adopts a probabilistic point of view where λ is modeled by a probability distribution Λ either Gaussian or log-Gaussian. In practice, model samples $\lambda_i \sim \Lambda$ can rarely be experimentally obtained, making the estimation process not straightforward. However, if the impact of Λ on some thermal-hydraulic QoIs predicted by the code is significant enough, an inverse statistical formulation can be used to estimate the parameters of Λ . This supposes that the mismatch between the available experimental QoIs and the corresponding code output predictions is due to the randomness of Λ . Let us consider the example of a heat transfer model impacting strongly a wall temperature in a pipe. In this case, the differences between the wall temperature measurements and the corresponding simulations could be used to get back to the uncertainty of the heat transfer model.

2.2. The statistical modeling

As explained previously, at least one experimental database is required to implement the CIRCE method. Throughout the paper, we will use the superscript f (meaning *field*) to refer to an experimental quantity. The various physical set-ups are synthesized in the matrix \mathbf{X}^f :

$$\mathbf{X}^f = [\mathbf{x}_1^f, \dots, \mathbf{x}_n^f]^T \in \mathcal{M}_{n,q}(\mathbb{R}). \quad (3)$$

with each site $\mathbf{x}_i^f \in \mathbb{R}^q$ being made up with the experimental values corresponding to the i th experiment. The experimental QoI at \mathbf{x}_i^f is denoted by $z_i^f \in \mathbb{R}$. The vector containing the whole QoIs is denoted by

$$\mathbf{z}^f = (z_1^f, \dots, z_n^f)^T \in \mathbb{R}^n. \quad (4)$$

Let $Y(\cdot)$ be a thermal-hydraulic system code being able to simulate \mathbf{z}^f . The CIRCE method relies on a statistical equation which relates \mathbf{z}^f to the corresponding simulations run at \mathbf{X}^f . The differences between the two are supposed to be realizations of n independent zero-mean Gaussian random variables. Hence, for $1 \leq i \leq n$,

$$z_i^f = Y(M_{\lambda_i}(\mathbf{x}_i^f)) + \epsilon_i \quad (5)$$

with λ_i being unobserved (we can say missing as well) and

$$\epsilon_i \sim \mathcal{N}(0, \sigma_{\epsilon_i}^2). \quad (6)$$

Equation (5) encompasses the case where the code outputs depend on several uncertain models, λ_i being a p -dimensional sample of the random vector $\Lambda := (\Lambda_1, \dots, \Lambda_p)^T$. Thus, $M_{\lambda_i}(\mathbf{x}_i^f)$ can be expanded on:

$$M_{\lambda_i}(\mathbf{x}_i^f) := (M_{\lambda_{i,1}}^1(\mathbf{x}_i^f), \dots, M_{\lambda_{i,p}}^p(\mathbf{x}_i^f)) \quad (7)$$

where $\lambda_{i,j}$ is the missing value applied to the j th reference model $M_{ref}^j(\cdot)$ for $1 \leq j \leq p$. The difference ϵ_i should be interpreted as a residual variable assessing the experimental uncertainty, although other source of errors attributed to the code may contribute to the mismatch as well. In Kennedy and O'Hagan (2001) a function $b(\mathbf{x}_i^f)$, called code discrepancy, is explicitly taken into account between the physical system and the computer code. We have omitted it in Equation (5) because the CIRCE method supposes that the code discrepancy is mainly due to the uncertainty affecting the physical models.

Let us point out that Equation (5) simply means that $Y(\cdot)$ depends on p uncertain models. This is not at all a composition of Y after $M_{\lambda_i}(\cdot)$. Thermal-hydraulic simulations follow an iterative process solving the fluid conservation equations in both time and space. The values of the reference physical models $M_{ref}(\cdot)$ are then changed over iterations, unlike the value of λ which remains constant all along the simulation. Equation (5) can therefore be rewritten under a reduced form:

$$z_i^f = Y_{\lambda_i}(\mathbf{x}_i^f) + \epsilon_i. \quad (8)$$

The CIRCE method relies on several other assumptions. First of all, the standard deviations σ_{ϵ_i} are assumed known for $1 \leq i \leq n$. Second, each component Λ_j of Λ follows either a Gaussian or a log-Gaussian probability distribution:

$$\Lambda_j = \mathcal{N}(m_j, \sigma_j^2) \quad \text{or} \quad \Lambda_j = \mathcal{LN}(m_j, \sigma_j^2), \quad 1 \leq j \leq p. \quad (9)$$

The last assumption, which is that the p variables Λ_j are independent from one another, is not compulsory, but highly recommended. For $1 \leq j \neq k \leq p$, we thus have

$$\text{Cov}(\Lambda_j, \Lambda_k) = 0. \quad (10)$$

In this way, we limit the number of parameters to be estimated to $2p$ instead of $3p$ if cross-covariance terms were estimated as well. Such probabilistic independence should not be confused with potential interactions occurring between the models within the code.

In the rest, we will use concise notations to refer to the p means and the p variances of Λ :

$$m = (m_1, \dots, m_p)^T \in \mathbb{R}^p \quad (11)$$

and

$$\sigma^2 = (\sigma_1^2, \dots, \sigma_p^2)^T \in \mathbb{R}^{+p}. \quad (12)$$

Before going ahead with statistical algorithms to estimate m and σ^2 , we quickly explain in the next paragraph what is the fundamental distinction between CIRCE and calibration of parameters.

2.3. Difference between CIRCE and calibration

The CIRCE method actually comes down to conducting probabilistic inversion. Based on the probability distribution of the differences between the simulations and the experimental QoIs, CIRCE aims to get back to the probability distribution of uncertain inputs which are multiplicative factors. Another example of probabilistic inversion can be found in Fu et al. (2015) where the probability distribution of Strickler coefficients is estimated in a flood risk problem. Although probabilistic inversion and calibration are both part of inverse UQ methods, the former aims to recover a probability distribution whereas the latter deals with parameter estimation. If calibration were performed instead of CIRCE, Equation (8) would be replaced by

$$z_i^f = Y_\lambda(\mathbf{x}_i^f) + \epsilon_i \quad (13)$$

where the value of the multiplicative factor(s) would be unchanged whatever \mathbf{x}_i^f , as done in Wu et al. (2018). According to this distinction, CIRCE actually deals with calibration of (m, σ^2) .

2.4. The linear setting

The implementation of the estimation procedure of the CIRCE method consists of linearizing the code output at a nominal value λ^* using a first order Taylor approximation, then calculating the Maximum Likelihood Estimate (MLE) of (m, σ^2) by means of a variant of the Expectation-Maximization (EM) algorithm (A. P. Dempster and Rubin, 1977). It is in fact quite frequent that thermal-hydraulic simulations move linearly with respect to the multiplicative factors λ in a large vicinity $\lambda \in V(\lambda^*) \subset \mathbb{R}^p$. For every input site $\mathbf{x}_i^f \in \mathbf{X}^f$, Equation (5) is then substituted by

$$z_i'^f = h^T(\mathbf{x}_i^f)\lambda'_i + \epsilon_i \quad (14)$$

where

- $\lambda'_i := \lambda_i - \lambda^* \sim \mathcal{N}(m - \lambda^*, \Sigma := \text{diag}(\sigma^2))$ is the missing model sample shifted of λ^* ,
- $h(\mathbf{x}_i^f) \in \mathbb{R}^p$ is the vector of partial derivatives of the code at λ^* ,
- $z_i'^f$ is the difference between the experimental QoI at \mathbf{x}_i^f and the simulation run at λ^* .

The location λ^* is chosen by default equal to $\mathbf{1}_p$, meaning that the linear approximation is made around the reference model.

Sometimes, the linearity assumption may be more accurate with respect to $\alpha = \log \lambda$. Equation (5) is then approximated around $\alpha^* = \log(\lambda^*)$ by

$$z_i'^f = h^T(\mathbf{x}_i^f)\alpha'_i + \epsilon_i \quad (15)$$

where

- $\alpha'_i = \alpha_i - \alpha^* \sim \mathcal{N}(m - \alpha^*, \Sigma)$ is the unobserved model log-samples shifted of α^* ,
- $h(\mathbf{x}_i^f) \in \mathbb{R}^p$ is the vector of partial derivatives of the code with respect to $\alpha^* = \log \lambda^*$.

The location α^* is chosen by default equal to $\mathbf{0}_p = \log \mathbf{1}_p$ and thus the log-linear approximation is still made around the reference model.

Both Models (14) and (15) are identifiable if and only if the rank of the partial derivatives matrix is equal to p . This matrix is denoted by

$$H = [h(\mathbf{x}_1^f), \dots, h(\mathbf{x}_n^f)]^T \in \mathcal{M}_{n,p}(\mathbb{R}). \quad (16)$$

A small condition number is also wanted to ensure reliability of estimates (Belsley et al., 1980). An EM-like algorithm, called ECME (Celeux et al., 2010), is then performed to calculate the MLE $(\hat{m}, \hat{\sigma}^2)$. Both EM and ECME are explained in details in Celeux et al. (2010). Confidence regions for (m, σ^2) , centered around $(\hat{m}, \hat{\sigma}^2)$, can be calculated by using either the samples generated by bootstrapping or the Fisher information matrix. Both of these methods are asymptotically valid.

The last stage of CIRCE, but not the least one, has to decide between the Gaussian distribution $\mathcal{N}(\hat{m}, \hat{\sigma}^2)$ and the log-Gaussian distribution $\mathcal{LN}(\hat{m}, \hat{\sigma}^2)$ where $(\hat{m}, \hat{\sigma}^2)$ are the estimates of Models (14) and (15) respectively. The choice goes in favor of the distribution that leads to the best linear approximation of the code outputs around λ^* or α^* respectively. If the Gaussian distribution is chosen for Λ_j , then the 95%-fluctuation interval of the multiplicative factor is given by

$$IF_{95\%}(\Lambda_j) = [\hat{m}_j - 1.96\hat{\sigma}_j, \hat{m}_j + 1.96\hat{\sigma}_j] \quad (17)$$

If the log-Gaussian distribution is chosen instead, then the 95%-fluctuation interval of the multiplicative factor is given by

$$IF_{95\%}(\Lambda_j) = [\exp(\hat{m}_j - 1.96\hat{\sigma}_j), \exp(\hat{m}_j + 1.96\hat{\sigma}_j)]. \quad (18)$$

Eventually, the validity of these results should be proven. First, the linearity assumption is to be checked throughout the chosen fluctuation interval above. Then, the structure of the predicted residuals should be analyzed to ensure that the distribution of them is not that different from the Gaussian distribution. Finally, what is referred to as *Envelop calculations* in the guidelines of CIRCE should be performed. The probability distribution Λ estimated by CIRCE is propagated through the code to check whether the resulting simulations can envelop the physical experiments \mathbf{z}^f .

In the next section, we lay out Bayesian inference of the CIRCE method. The paradigm behind it is that uncertain parameters are modelled by random variables. A prior distribution on (m, σ^2) is first specified, then the posterior distribution of (m, σ^2) is then computed using the Bayes theorem (see for example Ghosh et al. (2007) for an introductory book about Bayesian statistics).

3. The Bayesian inference of the CIRCE method

3.1. General principle

Without loss of generality, we now lay out the Bayesian equations related to Model (15) where Λ is specified as a log-Gaussian probability distribution. As the code is linearized at $\alpha^* = \log \lambda^*$, we deal with Bayesian estimation of $b := m - \alpha^*$ and σ^2 .

Let $\mathbf{A}' = [\alpha'_1, \dots, \alpha'_n]^T \in \mathcal{M}_{n,p}(\mathbb{R})$ and $\mathbf{z}'^f = (z'_1{}^f, \dots, z'_n{}^f)^T$ be respectively the matrix of the α^* -shifted missing values of the multiplicative factors and the vector of the α^* -shifted

experimental QoIs. Bayesian estimation of b and σ^2 starts by specifying a joint prior probability distribution on these unknown parameters, then sampling their posterior distribution conditional on \mathbf{z}'^f . Applying the Bayes theorem gives

$$\pi(b, \sigma^2 | \mathbf{X}^f, \mathbf{z}'^f) = \frac{\mathcal{L}(\mathbf{z}'^f | \mathbf{X}^f, b, \sigma^2) \pi(b, \sigma^2)}{\int_{\mathbb{R}^+} \int_{\mathbb{R}} \mathcal{L}(\mathbf{z}'^f | \mathbf{X}^f, b, \sigma^2) \pi(b, \sigma^2) db d\sigma^2} \quad (19)$$

where the numerator is the product between the likelihood related to Equation (15) and the prior distribution $\pi(b, \sigma^2)$, while the denominator is the normalization term. The likelihood in Equation (19) can be written as

$$\mathcal{L}(\mathbf{z}'^f | \mathbf{X}^f, b, \sigma^2) = \int_{\mathbb{R}^{n \times p}} \mathcal{L}^C(\mathbf{z}'^f, \mathbf{A}' | \mathbf{X}^f, b, \sigma^2) d\mathbf{A}' \quad (20)$$

with \mathcal{L}^C being the complete likelihood including the missing data \mathbf{A}' . The Bayes formula can be applied in a different way where \mathbf{A}' is estimated jointly with (b, σ^2) . Hence,

$$\pi(b, \sigma^2, \mathbf{A}' | \mathbf{X}^f, \mathbf{z}'^f) = \frac{\mathcal{L}(\mathbf{z}'^f | \mathbf{A}', \mathbf{X}^f, b, \sigma^2) \pi(\mathbf{A}', b, \sigma^2)}{\int_{\mathbb{R}^+} \int_{\mathbb{R}} \int_{\mathbb{R}^{n \times p}} \mathcal{L}(\mathbf{z}'^f | \mathbf{A}', \mathbf{X}^f, b, \sigma^2) \pi(\mathbf{A}', b, \sigma^2) d\mathbf{A}' db d\sigma^2} \quad (21)$$

The prior distribution can be expanded on

$$\pi(\mathbf{A}', b, \sigma^2) = \pi(\mathbf{A}' | b, \sigma^2) \pi(b, \sigma^2) \quad (22)$$

where $\pi(\mathbf{A}' | b, \sigma^2)$ is the density of the product of n Gaussian distributions having b and σ^2 as shared mean and variance. Equation (21) is more frequently used for such hierarchical Bayesian modeling that makes no distinction between missing data and parameters, both being unknown and modeled by random variables. Since the denominator in Equation (21) is unattainable, an MCMC algorithm shall be used to simulate the posterior distribution having $\pi(b, \sigma^2, \mathbf{A}' | \mathbf{X}^f, \mathbf{z}'^f)$ as density. Such an algorithm has the advantage of relying only on the numerator.

3.2. Gibbs sampling

A popular MCMC algorithm, referred to as the Gibbs sampler, has been introduced by Geman and Geman (1984) to compute posterior distributions in presence of unobserved data. This algorithm successively generates samples from every full conditional distribution by following a Markov-chain mechanism which has the theoretical property of converging to the targeted posterior distribution. It is described below applied to the sampling of $b, \sigma^2, \mathbf{A}' | \mathbf{X}^f, \mathbf{z}'^f$.

Gibbs sampling algorithm.

1. Set starting values: $(b(0), \sigma^2(0))$
2. Choose a number N_{mcmc} of iterations, then for $1 \leq k \leq N_{mcmc}$ generate in a loop:

$$\mathbf{A}'(k+1) \sim \mathbf{A}' | b(k), \sigma^2(k), \mathbf{z}'^f, \mathbf{X}^f \quad (23)$$

$$b(k+1) \sim b | \sigma^2(k), \mathbf{A}'(k+1), \mathbf{z}'^f, \mathbf{X}^f \quad (24)$$

$$\sigma^2(k+1) \sim \sigma^2 | b(k+1), \mathbf{A}'(k+1), \mathbf{z}'^f, \mathbf{X}^f \quad (25)$$

Equations (23), (24) and (25) are the full conditional distributions of \mathbf{A}' , b and σ^2 respectively. This algorithm generates samples from a Markov chain which theoretically converges to the posterior distribution (19). In practice, some diagnostics should be applied to check whether the chain has actually converged (see Section 3.5). If so, posterior samples $\{(b(k), \sigma^2(k))\}_i$ can be used for computing point estimates $(\hat{b}, \hat{\sigma}^2)$ as well as posterior credibility intervals. The posterior mean is equal to

$$(\hat{b}, \hat{\sigma}^2) = \mathbb{E}[b, \sigma^2 | \mathbf{X}^f, \mathbf{z}'^f]. \quad (26)$$

Another much used point estimate is the Maximum A Posteriori (MAP):

$$(\hat{b}, \hat{\sigma}^2) = \underset{b, \sigma^2}{\operatorname{argmax}} \pi(b, \sigma^2 | \mathbf{X}^f, \mathbf{z}'^f). \quad (27)$$

3.3. Computation of the full conditional posterior distributions

If the conjugate Gaussian-inverse gamma prior distribution is put on (b, σ^2) , the full conditional distributions (23), (24) and (25) are analytically tractable. This prior is defined by

$$\pi(b, \sigma^2) = \prod_{j=1}^p \pi(b_j, \sigma_j^2) = \prod_{j=1}^p \pi(b_j | \sigma_j^2) \pi(\sigma_j^2) \quad (28)$$

where for $1 \leq j \leq p$

$$\pi(b_j | \sigma_j^2) = \frac{\sqrt{a_j}}{\sqrt{2\pi}\sigma_j} \exp -\frac{a_j(b_j - \mu_j)^2}{2\sigma_j^2} \quad (29)$$

and

$$\pi(\sigma_j^2) = \frac{\gamma_j^{\psi_j}}{\Gamma(\psi_j)} \sigma_j^{2(-\psi_j-1)} \exp -\frac{\gamma_j}{\sigma_j^2}. \quad (30)$$

The Greek letter $\Gamma(\cdot)$ refers to the Euler gamma function and the values of the hyperparameters $\psi_j, \gamma_j, \mu_j, a_j$ are set depending on whether prior information is available on (b, σ^2) or not. In absence of prior information on (b, σ^2) , we expect to compute a data-dominated posterior distribution. In this context, the values $\mu_j = 0$, $a_j = \epsilon$, $\psi_j = \epsilon$ and $\gamma_j = \epsilon$ with ϵ being small are settings that make this prior vague (Spiegelhalter et al., 2004). However, as the posterior distribution of σ_j^2 puts a substantial probability mass around 0, a non negligible impact of the ϵ value on $\pi(b, \sigma^2 | \mathbf{z}'^f, \mathbf{X}^f)$ may be suspected (Gelman, 2006).

Theorem 1. *Using the Gaussian-inverse gamma (28) prior distribution, the full conditional distributions (23), (24) and (25) are equal to:*

$$b | \sigma^2, \mathbf{A}', \mathbf{z}'^f \sim \otimes_{j=1}^p \mathcal{N}\left(\frac{a_j}{a_j + n} \mu_j + \frac{n}{n + a_j} \bar{\alpha}'_j, \frac{\sigma_j^2}{n + a_j}\right) \text{ with } \bar{\alpha}'_j = \sum_{i=1}^n \alpha'_{i,j} \quad (31)$$

$$\sigma^2 | b, \mathbf{A}', \mathbf{z}'^f \sim \otimes_{j=1}^p \mathcal{IG}\left(\alpha_j + \frac{n}{2} + \frac{1}{2}, \frac{1}{2} \sum_{i=1}^n (\alpha'_{i,j} - m_j)^2 + \frac{a_j}{2} (m_j - \mu_j)^2 + \gamma_j\right) \quad (32)$$

$$\mathbf{A}' | b, \sigma^2, \mathbf{z}'^f \sim \otimes_{i=1}^n \mathcal{N}(S_i \nu_i, S_i) \quad (33)$$

where

$$S_i^{-1} = \frac{h(\mathbf{x}_i^f)h^T(\mathbf{x}_i^f)}{\sigma_{\epsilon_i}^2} + \Sigma^{-1} \in \mathbb{R}^{p \times p} \quad \text{with } \Sigma = \sigma^2 \mathbf{I}_p$$

and

$$\nu_i = \frac{h(\mathbf{x}_i^f)z_i^{\prime,f}}{\sigma_{\epsilon_i}^2} + \Sigma^{-1}b \in \mathbb{R}^p.$$

PROOF. See Appendix B.

The posterior distribution of (m, σ^2) is derived from that of (b, σ^2) by shifting of α^* the posterior samples $\{b(k)\}_k$.

3.4. A blocked Gibbs sampler

A slightly different algorithm can be performed instead of the pure Gibbs sampler.

Theorem 2. *The parameters (b, σ^2) are conditionnaly conjugated with respect to the unobserved samples \mathbf{A}' , meaning that the conditional distribution $b, \sigma^2 | \mathbf{A}', \mathbf{z}^{\prime,f}$ follows a Gaussian-inverse gamma distribution as well:*

$$\pi(b, \sigma^2 | \mathbf{A}', \mathbf{z}^{\prime,f}) = \pi(b | \sigma^2, \mathbf{A}', \mathbf{z}^{\prime,f}) \pi(\sigma^2 | \mathbf{A}', \mathbf{z}^{\prime,f}) \quad (34)$$

with

$$b | \sigma^2, \mathbf{A}' \sim \otimes_{j=1}^p \mathcal{N}\left(\frac{a_j \mu_j + n \bar{\alpha}'_j}{a_j + n}, \frac{\sigma_j^2}{a_j + n}\right) \quad (35)$$

and

$$\sigma^2 | \mathbf{A}' \sim \otimes_{j=1}^p \mathcal{IG}\left(\psi_j + \frac{n}{2}, \gamma_j + \frac{1}{2} \left(\sum_{i=1}^n (\alpha'_{i,j} - \bar{\alpha}'_j)^2 + \frac{a_j n (\bar{\alpha}'_j - \mu_j)^2}{a_j + n} \right)\right) \quad (36)$$

PROOF. Use the conjugency of the Gaussian-inverse gamma distribution (see for instance Murphy (2007) for details).

Therefore, the pure Gibbs sampler can be replaced by the blocked Gibbs sampler.

Blocked Gibbs sampling algorithm.

1. Set starting values: $(b(0), \sigma^2(0))$
2. Choose a number N_{mcmc} of iterations, then for $1 \leq k \leq N_{mcmc}$, generate in a loop:

$$\mathbf{A}'(k+1) \sim \mathbf{A}' | b(k), \sigma^2(k), \mathbf{z}^{\prime,f}, \mathbf{X}^f \quad (37)$$

$$b(k+1), \sigma^2(k+1) \sim b, \sigma^2 | \mathbf{A}'(k+1), \mathbf{z}^{\prime,f}, \mathbf{X}^f \quad (38)$$

This second algorithm, referred to as *substitution sampling* in Gelfand and Smith (1990), follows the hierarchical structure of Model (15). According to Diebolt and Robert (1994), it can converge faster to the stationary distribution than the pure Gibbs sampler. After starting both of these algorithms with values $b(0)$ and $\sigma^2(0)$ being far away from the support of the posterior distribution, we observed on an artificial example that the blocked Gibbs sampler moved faster to the region of high posterior probability.

3.5. Checking convergence of MCMC samplers

The convergence of the Gibbs samplers should be investigated in three ways as reported by Robert and Casella (1998):

1. convergence of the Markov chain to the stationary distribution, which is to check whether the distribution of the chain remains unchanged as iterations k increase.
2. convergence of averages. Let us consider, for instance, the posterior mean estimator of b :

$$\hat{b} = \frac{1}{N_{mcmc}} \sum_{k=1}^{N_{mcmc}} b(k) \quad (39)$$

Unlike traditional Monte Carlo (MC) estimates based on i.i.d. samples, the $\{b(k)\}_k$ are here correlated. Such MCMC estimators still converges to the posterior mean of b , though, it is less accurate than MC estimators. The convergence of averages actually deals with choosing N_{mcmc} so that (39) reaches a prescribed level of precision.

3. convergence to i.i.d. sampling, where we seek to pick up MCMC samples being as independent as possible.

A stationary test can be implemented to check the first goal. For the second goal, the so-called *effective sample size* is a useful indicator providing the number $N_{mc} < N_{mcmc}$ of hypothetical i.i.d. samples to be used to achieve the same accuracy than (39). The effective sample size is calculated from autocorrelation between posterior samples. The smaller the autocorrelation, the larger the effective sample size. The third goal, called sub-sampling, is still based on autocorrelation as consisting of picking up quasi-independent samples from the chain.

The CODA library of the R statistical software implements various indexes to monitor the convergence of MCMC sampling (Plummer et al., 2006). Some of those indexes will be applied in Section 5 for diagnosing the degree of convergence of the Gibbs samplers. For a deep comparison of convergence diagnostics, see for instance Cowles and Carlin (1996).

3.6. Bayesian fluctuation intervals

The primary interest of adopting the Bayesian setting is that the statistical uncertainty of (m, σ^2) can be taken into account in computing the fluctuation intervals of the multiplicative factors. These are derived from the predictive distribution of $\Lambda = (\Lambda_1, \dots, \Lambda_p)$ *a posteriori*, whose density is given by

$$\pi(\Lambda) = \int \pi(\Lambda|m, \sigma^2)\pi(m, \sigma^2|\mathbf{z}'^f)dm d\sigma^2. \quad (40)$$

where

$$\pi(\Lambda|m, \sigma^2) = \prod_{j=1}^p \pi(\Lambda_j|m_j, \sigma_j^2) \quad (41)$$

with $\pi(\Lambda_j|m, \sigma^2)$ being either a Gaussian or a log-Gaussian density depending on which linearity assumption we have selected. As $\pi(\Lambda)$ has no closed-form after integrating out the posterior distribution of (m, σ^2) , Monte-Carlo computation is needed to generate samples of Λ . To do so, generate $m(k), \sigma^2(k) \sim m, \sigma^2|\mathbf{z}'^f$ for $1 \leq k \leq N$ by the blocked Gibbs sampler, then generate $\lambda(k) \sim \Lambda|m(k), \sigma^2(k)$. For $1 \leq j \leq p$, this iterative process returns samples

$\lambda_j(1), \lambda_j(2), \dots, \lambda_j(N)$ which can be used to compute empirical quantiles of Λ_j . Let $q_{0.025}(\Lambda_j)$ and $q_{0.975}(\Lambda_j)$ be the 2.5% and the 97.5% quantiles of Λ_j . Then, for $1 \leq j \leq p$, an estimate of the 95% fluctuation interval of Λ_j is given by

$$IF_{95\%}(\Lambda_j) = [q_{0.025}(\Lambda_j), q_{0.975}(\Lambda_j)]. \quad (42)$$

The implementation of CIRCE or its Bayesian version can be subject to a strong user effect in constructing the matrix H of the partial derivatives (see Equation (16)). As thermal-hydraulic system codes tend to switch from a flow regime (or thermal regime) to another, the values of the finite differences can be tainted by the chosen increment. In addition, the resulting fluctuation intervals are likely to be large when the size of \mathbf{z}^f is small, which makes the linearity approximation unable to match properly the code outputs. Both of these limitations motivate us to tackle the general setting where the output of $Y(\cdot)$ does not move linearly against neither $\lambda \sim \Lambda$ nor $\alpha \sim \log \Lambda$.

4. The non linear setting

Let $\mathbf{A} = [\alpha_1, \dots, \alpha_n]^T \in \mathcal{M}_{n,p}(\mathbb{R})$ be the matrix of the missing log-samples of the multiplicative factors. As there is no longer linearization of the code output, we thus revert to the estimation of m (instead of b in the liner case). The Bayes theorem applied to Equation (8) with $\lambda = \exp \alpha$ gives

$$\pi(m, \sigma^2, \mathbf{A} | \mathbf{X}^f, \mathbf{z}^f) \propto \mathcal{L}(\mathbf{z}^f | \mathbf{A}, \mathbf{X}^f, m, \sigma^2) \pi(\mathbf{A} | m, \sigma^2) \pi(m, \sigma^2) \quad (43)$$

where $\pi(m, \sigma^2)$ is still a Gaussian-inverse gamma density. A blocked Gibbs sampler can then be run in a similar way to the linear case.

Blocked Gibbs sampling algorithm in the non linear setting.

1. Set starting values: $(m(0), \sigma^2(0))$
2. Choose a number N_{mcmc} of iterations, then for $1 \leq k \leq N_{mcmc}$ generate:

$$\mathbf{A}(k+1) \sim \mathbf{A} | m(k), \sigma^2(k), \mathbf{z}^f, \mathbf{X}^f \quad (44)$$

$$m(k+1), \sigma^2(k+1) \sim m, \sigma^2 | \mathbf{A}(k+1), \mathbf{z}^f, \mathbf{X}^f \quad (45)$$

The full conditional distribution (45) is unchanged compared to (38) (except we estimate m instead of b) whereas the probability density related to (44) is equal to

$$\begin{aligned} \pi(\mathbf{A} | m, \sigma^2, \mathbf{z}^f, \mathbf{X}^f) &= \prod_{i=1}^n \pi(\alpha_i | m, \sigma^2, z_i^f, \mathbf{x}_i^f) \\ &\propto \exp -\frac{1}{2} \sum_{i=1}^n \left[\frac{(z_i^f - Y_{\exp \alpha_i}(\mathbf{x}_i^f))^2}{\sigma_{\epsilon_i}^2} + (\alpha_i - m)^T \Sigma^{-1} (\alpha_i - m) \right] \end{aligned} \quad (46)$$

Unlike the linear setting, $\mathbf{A} | m, \sigma^2, \mathbf{z}^f, \mathbf{X}^f$ now depends on the computer code outputs $Y_{\exp \alpha_i}(\mathbf{x}_i^f)$ for $1 \leq i \leq n$. As a result, it does not have any explicit form and then MCMC methods are required, such as for instance a Metropolis-Hastings (MH) algorithm (Metropolis et al., 1953). This algorithm can generate quasi-independent samples $\{\mathbf{A}(k)\}_k$ whose the density is (46).

4.1. Metropolis-Hastings algorithm

The Gibbs sampler now includes an inner MH step which requires running n simulations of $Y(\cdot)$ at every iteration $1 \leq k \leq N_{mcmc}$. The MH algorithm relies on a proposal distribution which has to comply with some properties so that the Markov chain converges (Chib and Greenberg, 1995). As the density (46) is written as the product of the n marginal densities $\pi(\alpha_i|m, \sigma^2, z_i^f, \mathbf{x}_i^f)$ being independent of each other, we only need to focus on the way that the MH algorithm can generate samples from $\alpha_i|m, \sigma^2, z_i^f, \mathbf{x}_i^f$.

Metropolis-Hastings algorithm.

1. **Initialization:** Start with a value $\alpha_i(0)$;
2. **Loop:** Choose a number N_{mh} of iterations, then for $1 \leq s \leq N_{mh}$, sample:
 - $\alpha_i(new) \sim \pi_{prop}(\cdot|m(s), \sigma^2(s), \alpha_i(s))$ where $\pi_{prop}(\cdot|.)$ is a proposal density chosen by the user.
 - $\alpha_i(s+1) = \alpha_i(new)$ with probability equal to

$$p_{mh,i} = \min \left(1, \frac{\pi(\alpha_i(new)|m(s), \sigma^2(s), z_i^f, \mathbf{x}_i^f) \times \pi_{prop}(\alpha_i(s)|m(s), \sigma^2(s), \alpha_i(new))}{\pi(\alpha_i(s)|m(s), \sigma^2(s), z_i^f, \mathbf{x}_i^f) \times \pi_{prop}(\alpha_i(new)|m(s), \sigma^2(s), \alpha_i(s))} \right) \quad (47)$$

and $\alpha_i(s+1) = \alpha_i(s)$ with probability $1 - p_{mh,i}$.

Theorem 3. *By using a proposal density independent from the current state $\alpha_i(s)$, that is,*

$$\pi_{prop}(\alpha_i(new)|m(s), \sigma^2(s)) = \pi_{prop}(\alpha_i(new)|m(s), \sigma^2(s), \alpha_i(s)) \quad (48)$$

then the probability (47) can be simplified to

$$p_{mh,i} = \min \left(1, \frac{\pi(z_i^f|m(s), \sigma^2(s), \alpha_i(new), \mathbf{x}_i^f)}{\pi(z_i^f|m(s), \sigma^2(s), \alpha_i(s), \mathbf{x}_i^f)} \right) \quad (49)$$

where

$$\pi(z_i^f|m(s), \sigma^2(s), \alpha_i, \mathbf{x}_i^f) = \frac{1}{\sqrt{2\pi}\sigma_{\epsilon_i}} \exp -\frac{1}{2} \frac{(z_i^f - Y_{\exp \alpha_i}(\mathbf{x}_i^f))^2}{\sigma_{\epsilon_i}^2}. \quad (50)$$

PROOF. See Appendix C

By default, the proposal (48) can be chosen as a Gaussian density with mean $m(s)$ and variance $\sigma^2(s)$. The variance matrix should then be adjusted to improve mixing efficiency of the Markov chain in such a way that the acceptance rate is near 0.45 when $\alpha_i(\cdot) \in \mathbb{R}$ and tends to 0.25 as the dimension of the problem increases (Roberts et al., 1997). However, as the MH algorithm is here embedded in a Gibbs sampler, the own convergence of (46) is not of primary importance. In Section 5, we will choose $N_{mh} = 10$ while Müller (1991) even proposes $N_{mh} = 1$. The interest of such a simplification is stressed in Robert and Casella (1998) in which the authors say that

1. the stationary distribution of the Markov chain remains the same: $m, \sigma^2, \mathbf{A}|z^f, \mathbf{X}^f$,
2. a more exhaustive sampling of the full conditional distribution does not necessarily lead to a more precise estimate of the posterior distribution.

No matter the value of N_{mh} , the more time-consuming the simulations are, the more time-consuming the blocked Gibbs sampler will be. Once the simulations exceed few minutes, this algorithm is no longer practicable in a reasonable time because ten of thousands of iterations are often required for the convergence of the Markov chain. This handicap can be circumvented by replacing the code outputs by emulator predictions in Equation (46). In this work, we focused on the Gaussian process (GP) emulator which has been extensively used over years in the field of computer experiments (Sacks et al., 1989). It can deliver quick predictions of costly simulations as well as uncertainty bounds around them (see Santner et al. (2003) for a reference book about GPs).

4.2. The GP-based MH within Gibbs

Let us consider the code output $Y_\lambda(\mathbf{x}_i^f)$ as a function of $\lambda \in \mathcal{L}$ with \mathcal{L} being a subdomain of \mathbb{R}^p . The GP emulator is specified with a mean function $m_{\mathbf{x}_i^f}(\cdot)$ and a covariance function $K_{\mathbf{x}_i^f}(\cdot)$:

$$\widehat{Y}_{\mathbf{x}_i^f}(\lambda) \sim \mathcal{GP}(m_{\mathbf{x}_i^f}(\lambda), K_{\mathbf{x}_i^f}(\lambda, \lambda')) \quad (51)$$

In Equation (51) the positions of λ and \mathbf{x}_i^f have been reversed to make clear that the GP is fitted with respect to $\lambda \in \mathcal{L}$ at \mathbf{x}_i^f being fixed. Let us collect M model samples forming a design of experiments, denoted by

$$\mathbf{D}_M = [\lambda_1, \dots, \lambda_M]^T \in \mathcal{M}_{M,p}(\mathbb{R}) \quad (52)$$

The corresponding set of simulations run at \mathbf{x}_i^f is denoted by $Y_{\mathbf{x}_i^f}(\mathbf{D}_M)$. The prediction of the code output at a new location $\lambda \in \mathcal{L}$ is given by the random process conditioned on $Y_{\mathbf{x}_i^f}(\mathbf{D}_M)$, which is still Gaussian:

$$\widehat{Y}_{\mathbf{x}_i^f}^M(\lambda) := \widehat{Y}_{\mathbf{x}_i^f}(\lambda) | Y_{\mathbf{x}_i^f}(\mathbf{D}_M) \sim \mathcal{GP}\left(\mu_{\mathbf{x}_i^f}^M(\lambda), V_{\mathbf{x}_i^f}^M(\lambda, \lambda')\right) \quad (53)$$

where the two terms in the brackets are the conditional mean and variance respectively. Their mathematical forms obviously depend on both $m_{\mathbf{x}_i^f}(\cdot)$ and $K_{\mathbf{x}_i^f}(\cdot)$ (see Appendix A). From a Bayesian point of view, a GP emulator should be deemed as a non-parametric prior on the code outputs $Y_{\mathbf{x}_i^f}(\lambda)$ and, therefore, Equation (53) is sometimes referred to as the posterior GP (Currin et al., 1991).

The mean function in Equation (51) is commonly assumed as either constant or the product between a vector of regression functions and a vector $\beta_i := \beta_{\mathbf{x}_i^f}$ of regression parameters:

$$m_{\mathbf{x}_i^f, \beta_i}(\lambda) = \beta_i \quad \text{or} \quad m_{\mathbf{x}_i^f, \beta_i}(\lambda) = H_i(\lambda)^T \beta_i \quad (54)$$

The covariance function can be calculated as the product between a scale parameter $\sigma_i^2 := \sigma^2(\mathbf{x}_i^f) \in \mathbb{R}^+$ and a correlation function indexed by a vector of correlation lengths $l_i := l(\mathbf{x}_i^f) \in \mathbb{R}^p$. Hence,

$$K_{\mathbf{x}_i^f, \sigma_i^2, l_i}(\lambda, \lambda') = \sigma_i^2 C_{\mathbf{x}_i^f, l_i}(\lambda, \lambda'). \quad (55)$$

Various correlation functions can be used to fit GP emulators, such as those of Matérn type on which we focus because of their flexibility. If $p = 1$, let us define $\delta\lambda = |\lambda - \lambda'|$ with

$\lambda, \lambda' \in \mathcal{L} \subset \mathbb{R}$ and $\Gamma(\cdot)$ and $K(\cdot)$ being the Gamma and Bessel functions respectively. The one dimensional Matérn function is written as

$$C_{\mathbf{x}_i^f, l_i}^{1d, \nu}(\delta\lambda) = \frac{1}{\Gamma(\nu)} \left(\sqrt{\nu} \frac{\delta\lambda}{l_i} \right)^\nu K_\nu \left(2\sqrt{\nu} \frac{\delta\lambda}{l_i} \right) \quad (56)$$

with l_i and ν being a correlation length and a smoothness parameter respectively. This function is stationary and quantifies to which extent the code output $Y_{\mathbf{x}_i^f}(\lambda)$ is likely to be close to $Y_{\mathbf{x}_i^f}(\lambda')$ against the distance $\delta\lambda$. The larger ν , the smoother the correlation. If $p \geq 2$, a multi-dimensional Matérn function relies on a distance in \mathbb{R}^p written as

$$\delta\lambda = \sqrt{\left[\sum_{j=1}^p \left(\frac{\delta\lambda_j}{l_{i,j}} \right)^2 \right]} \quad (57)$$

with $\lambda = (\lambda_1, \dots, \lambda_p)^T$ and $l_i = (l_{i,1}, \dots, l_{i,p})^T$. Then, an isotropic Matérn function is constructed by replacing $\delta\lambda$ by (57) into Equation (56):

$$C_{\mathbf{x}_i^f, l_i}^\nu(\delta\lambda) = C_{\mathbf{x}_i^f, l_i}^{1d, \nu} \left(\sqrt{\left[\sum_{j=1}^p \left(\frac{\delta\lambda_j}{l_{i,j}} \right)^2 \right]} \right). \quad (58)$$

In real problems, ν is often chosen according to the smoothness of the code outputs whereas the hyperparameters β_i , σ_i^2 and l_i are estimated from $Y_{\mathbf{x}_i^f}(\mathbf{D}_M)$ as part of the theorem below. This theorem provides an approximation of the density (46) where the thermal-hydraulic simulations are substituted for the mean and variance of the posterior GP.

Theorem 4. *Let us assume that one GP emulator is constructed per site $\mathbf{x}_i^f \in \mathbf{X}^f$ for $1 \leq i \leq n$. The whole set of simulations for fitting the n GP emulators denoted by*

$$Y(\mathbf{D}_M) := \cup_{i=1}^n Y_{\mathbf{x}_i^f}(\mathbf{D}_M). \quad (59)$$

Based on Equation (53), a GP-based approximation of the probability density (46) is written as

$$\begin{aligned} \pi(\mathbf{A}|Y(\mathbf{D}_M), m, \sigma^2, \mathbf{z}^f) &\propto \prod_{i=1}^n \frac{1}{\sqrt{\sigma_{\epsilon_i}^2 + V_{\mathbf{x}_i^f, \hat{l}_i, \hat{\sigma}_i^2}^M(\exp(\alpha_i), \exp(\alpha_i))}} \times \\ &\exp -\frac{1}{2} \sum_{i=1}^n \left[(z_i^f - \mu_{\mathbf{x}_i^f, \hat{\beta}_i, \hat{l}_i}^M(\exp(\alpha_i))^T (\sigma_{\epsilon_i}^2 + V_{\mathbf{x}_i^f, \hat{l}_i, \hat{\sigma}_i^2}^M(\exp(\alpha_i), \exp(\alpha_i)))^{-1} \right. \\ &\quad \left. (z_i^f - \mu_{\mathbf{x}_i^f, \hat{\beta}_i, \hat{l}_i}^M(\exp(\alpha_i)) + (\alpha_i - m)^T \Sigma^{-1}(\alpha_i - m)) \right] \quad (60) \end{aligned}$$

with $\hat{\beta}_i, \hat{l}_i, \hat{\sigma}_i^2$ being point estimates of the hyperparameters.

PROOF. Carry out a Bayesian modular approach (see Appendix D)

The probability density (60) is much cheaper than (46) because it no longer depends on the computer code outputs. The MH step explained previously can then be easily adapted to sample (60) instead of (46). As a result, we can run a *GP-based MH within Gibbs* algorithm

which consists of sampling the two conditional distributions (60) and (38) one after the other. The more the GP emulators can yield accurate predictions of the thermal-hydraulic simulations, the closer (60) should be to (46) and, therefore, the closer the GP-based posterior distribution should be to the exact posterior distribution (43).

In what follows, we present the COSI database that we will use to estimate two multiplicative factors applied to two condensation models at the safety injections.

5. Application to COSI tests

5.1. Description

The COSI⁸ database has been established from a SET facility which reproduces the cold leg and the emergency core cooling injection of a nuclear power plant with a power and volumic scale of 1/100. This facility allows to characterize two heat transfer phenomena to which the two multiplicative factors Λ_1 and Λ_2 are referred:

- Λ_1 is applied to the condensation created on the free surface far from the injection (Janicot and Bestion, 1993),
- Λ_2 is applied to the condensation due to the turbulent mixing in the vicinity of the injection jet (Gaillard et al., 2015).

The COSI facility is composed of:

- a cold leg,
- an emergency core cooling injection,
- a downcomer,
- a boiler to regulate the pressure in the test facility.

We have considered steady-state tests. Various thermal-hydraulic conditions $\{\mathbf{x}_i^f \in \mathbb{R}^4\}_i$ have been tested, such that:

- water height in the cold leg is between 0 and 60%,
- injection temperature between is 20 and 80 degrees Celsius,
- pressure in the test facility is between 20 and 70 bars,
- injection flow rate is between 0.1 and 0.6 kg/s.

The instrumentation is composed by thermocouples in the cold leg as well as a boiler flow rate measuring device to follow the temperature evolution in the liquid layer and the condensation flow rate in the facility respectively. The vector \mathbf{z}^f will be composed by $n = 50$ condensation flow rate values with respect to various input conditions \mathbf{x}_i^f for $1 \leq i \leq n$. The standard deviation of z_i^f is equal to $\sigma_{\epsilon_i} = 10^{-4}$ for any $1 \leq i \leq n = 50$.

⁸COndensation at the Safety Injections

5.2. Bayesian estimation using the linear approximations

First, the CIRCE method described in Section 2 has been implemented to the COSI tests. Both Gaussian and log-Gaussian parametrizations have been tested (see Equation 14 and 15 respectively). In this context, the latter gives the best approximation of the code output and thus Λ_1 and Λ_2 follow each a log-Gaussian distribution. Applying the CIRCE method yields the following biases:

$$(\hat{b}_1, \hat{b}_2) = (0.85, -0.78). \quad (61)$$

As these values are far away from 0, the linear approximation made at $\alpha^* = (0, 0)$ may be poor in the vicinity of (\hat{b}_1, \hat{b}_2) . A way of improving the robustness of the method is to make successive linearizations until small biases are obtained. This is referred to as the iterative CIRCE method (Nouy and de Crécy, 2017). For the COSI tests, four iterations have been made, the last being at $\alpha^* = (\log 1.73, \log 0.48) = (0.55, -0.73)$. The biases computed by CIRCE at this α^* are equal to

$$(\hat{b}_1, \hat{b}_2) = (0.008, -0.019). \quad (62)$$

Equation (18) gives the resulting fluctuation intervals of Λ_1 and Λ_2 :

$$IF_{95\%}(\Lambda_1) = [0.84, 3.61] \quad ; \quad IF_{95\%}(\Lambda_2) = [0.11, 1.98] \quad (63)$$

We have applied the CIRCE method as a preliminary step so that the linear approximation of the code output is as accurate as possible around (\hat{b}_1, \hat{b}_2) . Afterwards, we run the blocked Gibbs sampler laid out in Section 3 through an executable C++ macro relying on the TDataServer class of the Uranie platform (Blanchard et al., 2018). A number of 3×10^6 MCMC samples has been generated in a few minutes and stored in an object *TTree* of this class. Then, we applied the Geweke diagnostic to determine a period of iterations, called burn-in, after which the Markov chain has likely converged to the posterior distribution (Geweke, 1992). The idea is then to compare the first 10% samples of the chain with the 50% last samples in terms of mean estimate. If the Z-test for mean comparison is passed, then it is likely that the chain has reached its stationary distribution somewhere in the first part. The four p values for m_1 , m_2 , σ_1^2 and σ_2^2 calculated with the *geweke.diag()* function from the CODA package are all above 0.05 and then no evidence of non-convergence in the first part has been detected at this level of significance. As a result, we saved the last 2.7×10^6 samples to compute the posterior means, which are equal to $\hat{b}_1 \approx -0.0028$, $\hat{b}_2 \approx 0.0049$, $\hat{\sigma}_1^2 \approx 0.1577$ and $\hat{\sigma}_2^2 \approx 0.5651$. By moving of α^* the posterior distribution of (b_1, b_2) , we derived the posterior distribution of (m_1, m_2) and then $\hat{m}_1 = 0.5447$ and $\hat{m}_2 = -0.7208$. The effective sample size (e.s.s.) values of the marginal posterior distributions of m_1 , m_2 , σ_1^2 , σ_2^2 were computed by the *effectiveSize()* function. These values allowed us to compute the 95% confidence intervals of the previous estimates:

$$IC_{95\%}(\hat{m}_1) = [0.5427, 0.5467] \quad ; \quad IC_{95\%}(\hat{m}_2) = [-0.7253, -0.7164] \quad (64)$$

and

$$IC_{95\%}(\hat{\sigma}_1^2) = [0.1569, 0.1584] \quad ; \quad IC_{95\%}(\hat{\sigma}_2^2) = [0.5618, 0.5684] \quad (65)$$

After subsampling of the total chain, every 100th sample has been picked up. Figures 1 and 2 display such quasi-independent samples of the posterior distribution of (m_1, m_2) and (σ_1^2, σ_2^2) respectively. The posterior crossed plots between m_1 and m_2 and between σ_1^2 and σ_2^2

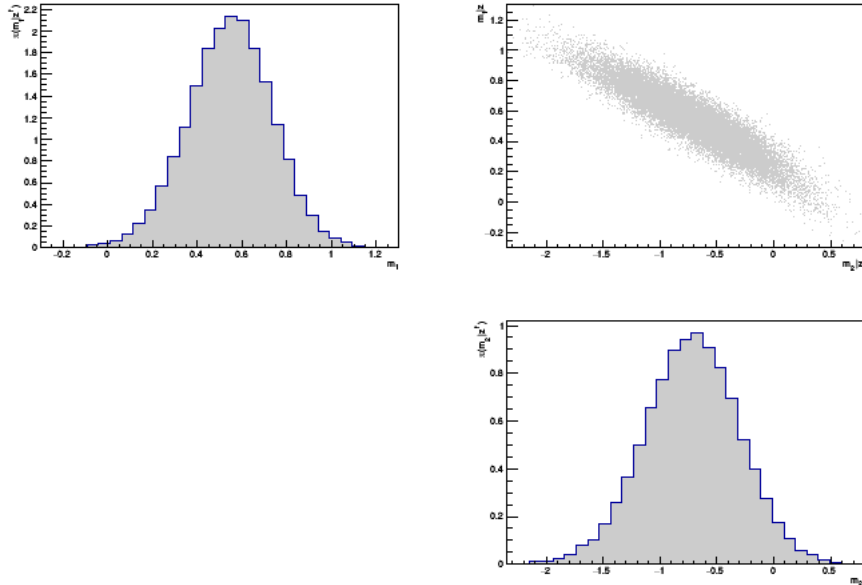
are displayed because their correlation is significant (equal to -0.87 and -0.57 respectively). The strong negative correlation between m_1 and m_2 shows that a positive bias for Λ_1 can be compensated by a negative bias for Λ_2 , which is coherent with the physical expertise about these two condensation models. Let us point out that the correlation between m_j and σ_j^2 ($j = 1, 2$) is not displayed because it is negligible. Then, the predictive distribution of $\Lambda = (\Lambda_1, \Lambda_2)$ has been sampled in order to derive the 95% fluctuation intervals of Λ_1 and Λ_2 (see Section 3.6):

$$IF_{95\%}(\Lambda_1) = [0.69, 3.97] \quad ; \quad IF_{95\%}(\Lambda_2) = [0.08, 2.43] \quad (66)$$

These intervals are more spread out than those given by Equation (63) because the uncertainty of (m, σ^2) is taken into account in their computation.

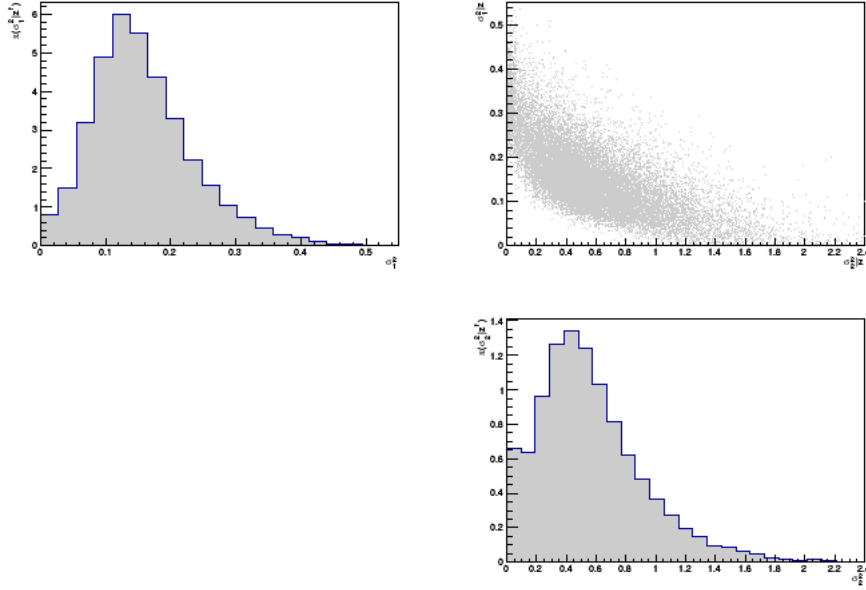
The last step is to check whether every linear approximation made at α_* is accurate enough to ensure that the previous results are reliable. We have seen that the agreements between the linear approximations and the code outputs are quite poor in the tails of the intervals (66), which motivates to tackle the non linear setting.

Figure 1: *Posterior distribution of (m_1, m_2) . This figure displays 2.7×10^4 quasi-independent samples (obtained after thinning of the entire chain to reduce the autocorrelation).*



Remark 1. As discussed in Section 3.3, we have used the diffuse Gaussian-inverse gamma prior distribution with $\epsilon = 10^{-2}$. We can see that the posterior distribution of σ_2^2 puts a significant probability mass close to 0. This is due to the prior density which is unbounded when σ_2^2 tends to 0.

Figure 2: Posterior distribution of (σ_1^2, σ_2^2) . This figure displays 2.7×10^4 quasi-independent samples (obtained after thinning of the entire chain to reduce the autocorrelation).



5.3. Bayesian estimation in the non linear setting

5.3.1. Fitting the GP emulators

As the CATHARE 2 simulations take some minutes, we need to run a GP-based MH within Gibbs sampler. This algorithm, whose principle is explained in Section 4, requires fitting one GP emulator per input site $\mathbf{x}_i^f \in \mathbf{X}^f$ ($1 \leq i \leq 50$) by means of the learning simulations $Y_{\mathbf{x}_i^f}(\mathbf{D}_M)$. The way used to construct \mathbf{D}_M is described hereafter:

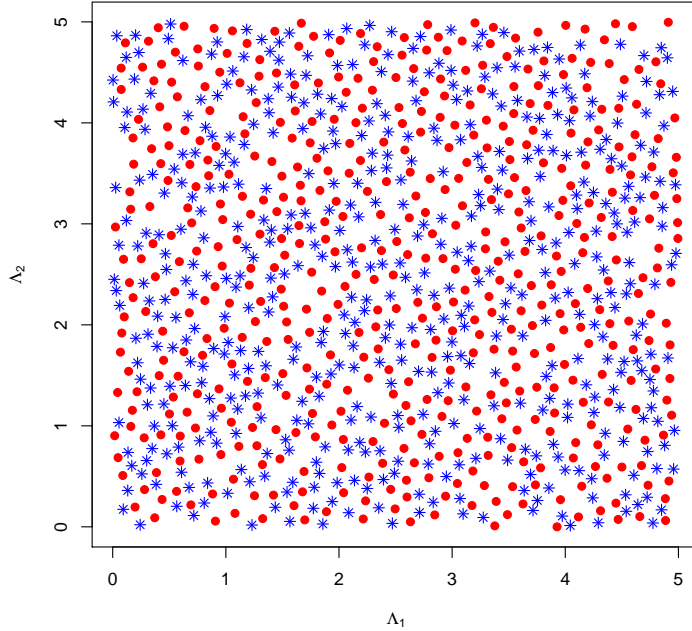
1. construction of \mathbf{D}_{2M} as a Space Filling Design (SFD) with $2M$ locations $\lambda_j \in \mathcal{L}$ ($1 \leq j \leq M$). The method *maximinSA_LHS* from the R library Dice Design has been used to do that;
2. construction of \mathbf{D}_M by using the *wspDesign* function from the same library. This can take out M simulations of \mathbf{D}_{2M} in such a way that the remaining M simulations form a SFD of \mathcal{L} ;
3. construction of $\mathbf{D}_M^{test} = \mathbf{D} - \mathbf{D}_M$ that we will use as a testing design to check the reliability of the GP emulators:

$$\mathbf{D}_M^{test} = [\lambda_1^{test}, \dots, \lambda_M^{test}]^T \in \mathcal{M}_{M,p}(\mathbb{R}). \quad (67)$$

The choice of \mathcal{L} should depend on the values that the two multiplicative factors can take. Based on physical expertise on the two condensation models, we have chosen $\mathcal{L} := (0, 5) \times (0, 5)$. By following the above steps, a learning and a testing design each with $M = 500$ locations have been constructed together. These are displayed in Figure 3.

Every GP emulator at \mathbf{x}_i^f ($1 \leq i \leq 50$) has been fitted by the *Modeler* module of the URANIE platform. We have used the correlation function (58) along with a constant mean $m_{\mathbf{x}_i^f, \beta_i}(\cdot) = \beta_i$. Several values of ν have been tested including $\nu = 5/2$, $\nu = 3/2$ and $\nu = 1/2$.

Figure 3: Red dots \mathbf{D}_M are locations used for learning the GP emulators. Blue stars \mathbf{D}_M^{test} are locations used for testing the reliability of predictions all over $\mathcal{L} = (0, 5) \times (0, 5)$.



The hyperparameters β_i , σ_i^2 and $l_i = (l_{i,1}, l_{i,2})^T$ have been estimated by maximizing their likelihood with respect to the learning simulations $Y_{\mathbf{x}_i^f}(\mathbf{D}_M)$ (see Appendix E). After that, both the predictive mean and variance in Equation (53) can be evaluated at any $\lambda \in \mathcal{L}$. In order to check their reliability throughout \mathcal{L} , we have computed the prediction coefficient $Q_{test}^2(\mathbf{x}_i^f)$ as well as the standardized prediction errors. These indicators are helpful to assess, respectively, the goodness-of-fit of the GP predictions and the relevance of the chosen correlation function. The prediction coefficient is written as

$$Q_{test}^2(\mathbf{x}_i^f) = 1 - \frac{\sum_{j=1}^M (Y_{\mathbf{x}_i^f}(\lambda_j^{test}) - \mu_{\mathbf{x}_i^f, \hat{\beta}_i, \hat{l}_i}^M(\lambda_j^{test}))^2}{\sum_{j=1}^M (Y_{\mathbf{x}_i^f}(\lambda_j^{test}) - \bar{Y}_{\mathbf{x}_i^f}^{test})^2} \quad (68)$$

with $\bar{Y}_{\mathbf{x}_i^f}^{test}$ being the mean of the M simulations of \mathbf{D}_M^{test} . Same formula can be applied to the locations of \mathbf{D}_M , though based on leave one out (loo) predictions:

$$Q_{loo}^2(\mathbf{x}_i^f) = 1 - \frac{\sum_{j=1}^M (Y_{\mathbf{x}_i^f}(\lambda_j) - \mu_{\mathbf{x}_i^f, \hat{\beta}_i, \hat{l}_i}^{M-j}(\lambda_j))^2}{\sum_{j=1}^M (Y_{\mathbf{x}_i^f}(\lambda_j) - \bar{Y}_{\mathbf{x}_i^f})^2} \quad (69)$$

with $\mu_{\mathbf{x}_i^f, \hat{\beta}_i, \hat{l}_i}^{M-j}(\cdot)$ being the predictive mean μ computed with respect to the M learning simulations except the j th and $\bar{Y}_{\mathbf{x}_i^f}$ is the mean of the M simulations of \mathbf{D}_M .

For $1 \leq i \leq 50$, almost all the values of $Q_{loo}^2(\mathbf{x}_i^f)$ and $Q_{test}^2(\mathbf{x}_i^f)$ are above 0.99 regardless of the value of ν . The predictive mean of the GP emulators is thus not affected by ν in terms of goodness of fit. However, we have seen that the larger ν , the smaller the predictive variance. We have then calculated the standardized prediction errors (s.p.e.), both by leave-one-out cross validation from \mathbf{D}_M and from \mathbf{D}_M^{test} . The value of ν can be judged as being appropriate when the empirical distribution of the s.p.e. matches that of the standard Gaussian distribution Φ as much as possible. For every GP at \mathbf{x}_i^f ($1 \leq i \leq 50$), we derived the percentages of the s.p.e which are outside the 95% bilateral interval of Φ :

$$IF_{95\%}(\Phi) = [-1.96, 1.96] \quad (70)$$

Figure 4 displays the distribution of those percentages over \mathbf{X}^f respectively for $\nu = 5/2$, $\nu = 3/2$ and $\nu = 1/2$. We compared them to the theoretical 5% remaining in the tails of Φ . For $\nu = 5/2$, we obtained on average 10% of errors calculated from \mathbf{D}_M falling outside $IF_{95\%}(\Phi)$ and 14.5% from \mathbf{D}_M^{test} . For $\nu = 3/2$, we obtained 3.6% and 4.5% respectively. For $\nu = 1/2$ we obtained 1.1% and 1% respectively. The best agreement with the theoretical 5% is thus reached with $\nu = 3/2$.

Several GP-based MH within Gibbs algorithms are then run to measure whether or not the choice of ν modifies the shape of the resulting GP-based posterior distribution:

1. Setting 1: $\nu = 5/2$. As we have just seen, the GP emulators here underestimate the predictive variance;
2. Setting 2: $\nu = 3/2$. The agreement with (70) is good on average over \mathbf{X}^f . However, there are a few sites \mathbf{x}_i^f at which the 5% threshold is significantly exceeded (see Figure 4 upper right);
3. Setting 3: mix between $\nu = 3/2$ and $\nu = 1/2$ depending on \mathbf{x}_i^f . The value $\nu = 1/2$ is used instead $\nu = 3/2$ for sites at which the percentage of errors from \mathbf{D}_M^{test} falling outside (70) is larger than 5%. This is the most conservative option in that the predictive variances are not likely to be underestimated.

Like in the linear study, we have collected 3×10^6 samples from the GP-based MH within Gibbs algorithm. As the autocorrelation is much stronger than it was in the linear case, showing a poor mixing of the Markov chain, we have run four chains in parallel starting from different $(m(0), \sigma^2(0))$. In Setting 1, only the second chain passed the Geweke testing at level 5%. In Setting 2, the third and fourth chains passed it. In Setting 3, all the chains passed it except the fourth one. We have also applied the Brooks-Gelman statistic to check whether the four chains all seem to converge towards the posterior distribution (Brooks and Gelman, 1998). This statistic computes the ratio of the between-chains variance to the within-chain variance for each parameter m_1 , m_2 , σ_1^2 , σ_2^2 . A rule of thumb to declare convergence is that the ratio is down 1.10, but more generally the closest the ratio to 1, the most likely the convergence. For each of the three settings, the ratio is rapidly dropping below 1.05 as iterations increase. In Setting 1, however, the ratio for σ_2^2 rises to 1.09 after 10^6 iterations, then decreases again to 1 beyond 2×10^6 . This is probably due to poor mixing of the chains. Nevertheless, we can conclude there is no evidence for non convergence of any chains.

Among the chains that passed the Geweke testing in each of the three settings, the one having the highest effective sample size after cutting off the burn-in period has been selected. Tables 1 and 2 summarize the posterior means of m_1 , m_2 and σ_1^2 , σ_2^2 respectively. We could

Table 1: Posterior mean estimates of m_1 and m_2 and their corresponding confidence interval

GP emulator type	$\widehat{\mathbb{E}}[m_1 \mathbf{z}^f]$	$IC_{95\%}(\mathbb{E}[m_1 \mathbf{z}^f])$	$\widehat{\mathbb{E}}[m_2 \mathbf{z}^f]$	$IC_{95\%}(\mathbb{E}[m_2 \mathbf{z}^f])$
Setting 1	0.7602	[0.7518, 0.7686]	-1.5071	[-1.5353, -1.4789]
Setting 2	0.6963	[0.6863, 0.7064]	-1.3814	[-1.4145, -1.3484]
Setting 3	0.6959	[0.6876, 0.7043]	-1.3706	[-1.4003, -1.3408]

Table 2: Posterior mean estimates of σ_1^2 and σ_2^2 and their corresponding confidence interval

GP emulator type	$\widehat{\mathbb{E}}[\sigma_1^2 \mathbf{z}^f]$	$IC_{95\%}(\mathbb{E}[\sigma_1^2 \mathbf{z}^f])$	$\widehat{\mathbb{E}}[\sigma_2^2 \mathbf{z}^f]$	$IC_{95\%}(\mathbb{E}[\sigma_2^2 \mathbf{z}^f])$
Setting 1	0.1592	[0.1564, 0.1621]	0.8883	[0.8564, 0.9203]
Setting 2	0.1528	[0.1463, 0.1593]	1.4785	[1.4305, 1.5265]
Setting 3	0.1474	[0.1420, 0.1528]	1.5365	[1.4877, 1.5852]

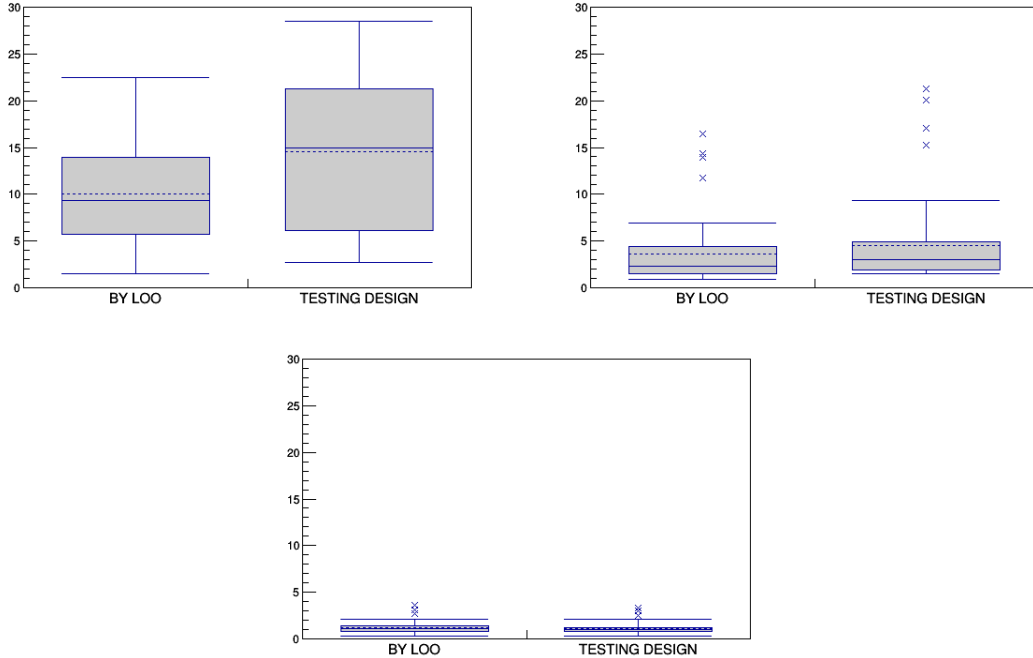
expect that the smaller the ν value, the larger the posterior samples of σ_1^2 and σ_2^2 , since the predictive variances of the GP emulators are increased between Setting 1 and Setting 2 and 3. As we can see in Table 2, only the posterior mean of σ_2^2 is actually increased. Table 3 displays the fluctuation intervals of Λ_1 and Λ_2 , showing that of Λ_2 is much more spread out in Settings 2 and 3 than in Setting 1 whereas that of Λ_1 does not change much (and even a little bit narrower). Although both models interact each other in predicting the overall condensation flow rate, a preliminary sensitivity analysis of the COSI tests has shown that Λ_2 is applied to the condensation model which mainly impacts the overall condensation flow rate. This factor may thus be more affected by changes in (60). Besides, if conservative fluctuation intervals are wanted, Setting 2 or even more Setting 3 should be preferred over Setting 1 because this last one is based on predictive variances of the GP emulators being underestimated.

If the predictive variances of the GP emulators are larger than or comparable to the variances $\sigma_{\epsilon_i}^2$ of the experimental quantities \mathbf{z}^f , then the values of the GP-based conditional distribution (60) are likely to be very different than those taken by (46). For the COSI tests, the predictive variance of the GP emulators is on average about equal to 10^{-7} in Settings 2 and 3 while the variance of the experimental condensation flow rates is equal to 10^{-8} . As a consequence, we cannot draw any conclusion about the scale of the difference between the fluctuation intervals reported in Table 3 and those which would have been computed from the exact posterior distribution if the CATHARE 2 simulations had been sufficiently cheap.

Table 3: 95% fluctuation intervals of Λ_1 and Λ_2

GP emulator type	$IF_{95\%}(\Lambda_1)$	$IF_{95\%}(\Lambda_2)$
Setting 1	[0.82, 4.80]	[0.02, 1.59]
Setting 2	[0.73, 4.44]	[0.01, 2.93]
Setting 3	[0.76, 4.39]	[0.01, 3.03]

Figure 4: *Distribution over \mathbf{X}^f of the percentage of standardized prediction errors that are not covered by the 5% bilateral fluctuation interval of the standard Gaussian distribution. Boxplots are thus made with 50 percentage values. Upper left: $\nu = 5/2$. Upper right: $\nu = 3/2$. Bottom: $\nu = 1/2$*



6. Conclusions

6.1. Summary

The paper has laid out a Bayesian methodology to quantify the uncertainty of the closure relationships integrated into thermal-hydraulic system codes. This work should be received as the Bayesian counterpart of the CIRCE method in that the joint posterior probability distribution of (m, σ^2) is computed instead of a point estimate $(\hat{m}, \hat{\sigma}^2)$. The interest in doing so is that the statistical uncertainty of $(\hat{m}, \hat{\sigma}^2)$ is now taken into account in computing the fluctuation intervals of the multiplicative factors applied to the closure relationships. In addition, we have tackled the extended Bayesian framework where the linear assumption of the code output with respect to the factors has been dropped. As a consequence, the fluctuation intervals are expected to be more spread out than those calculated with the original CIRCE method, which is particularly wise within BEPU studies where an higher degree of conservatism is expected in the determination of uncertainties.

An efficient MCMC algorithm, referred to as the Gibbs sampler, has been implemented both in the linear and non linear settings to simulate the posterior distribution of (m, σ^2) . Unfortunately, the cost of this algorithm strongly increases as the thermal-hydraulic simulations are moderately time consuming. For this reason, a cheaper posterior distribution has been constructed in the non linear setting by emulating the computer code. We have opted for the Gaussian process (GP) emulator which is particularly suited for computer experiments. Unlike other surrogates, such as neural networks, polynomial chaos expansion, it can interpolate

the learning simulations as well as yield Gaussian predictions of the code outputs at any other location. The GP-based posterior distribution that we have sampled derives from a GP-based Gibbs algorithm in which the full conditional posterior distribution of the (log)-values of the multiplicative factors depends on both the predictive mean and variance of the GP emulators. A great attention has been paid on the choice of the correlation so that the smoothness of the CATHARE 2 simulations in predicting the COSI tests is captured as best as possible. Several Matérn correlation functions have been tested with various smoothness parameters including $\nu = 0.5$, $\nu = 1.5$, $\nu = 2.5$. The smaller ν , the less smooth the Gaussian process trajectories. The values $\nu = 0.5$ and $\nu = 1.5$ yielded much more robust predictions of the condensation flow rate than the value $\nu = 2.5$ that underestimated the predictive variance. The fluctuation intervals computed with $\nu = 2.5$ (Setting 1) are different than those computed with a more suited $\nu = 1.5$ (Setting 2) or even a more conservative option (Setting 3).

The more the GP predictions match the code outputs, the closer the GP-based posterior distribution is expected to match the exact posterior distribution (43). However, it remains challenging to quantify the actual gap between both of these distributions. While this question remains open to our knowledge, a practical way to ensure that it is negligible would consist in increasing the number of learning simulations until the GP-based posterior distribution remains unchanged. This kind of stability could be achieved under two conditions. First, the variance of the GP predictions in (60) should be negligible with respect to the experimental uncertainty. Second, the reliability of the GP predictions should be ensured. If both are fulfilled, then the density (60) will likely take values quite close to (46) and, as a consequence, the GP-based posterior distribution will likely be close to (43). From a theoretical point of view, these two conditions are asymptotically ensured due to the consistency of the GP emulator, meaning that predictive means and variances converge towards the code outputs and 0 respectively. This property of consistency has been utilized in Damblin et al. (2018) to prove that the GP-based posterior distribution converges to the exact posterior distribution (43) in a certain sense.

6.2. Future works

According to the previous discussion, enhancing the accuracy of the GP emulators should be aimed for. This would be done by increasing the number of learning simulations so that the predictive variance significantly declines against the variance of the experimental condensation flow rate. However, the computational cost of the GP-based Gibbs algorithm would increase because the more the number of learning simulations for fitting the GP emulators, the more expensive $\mu_{\mathbf{x}_i^f}(\cdot)$ and $V_{\mathbf{x}_i^f}(\cdot)$ would be within the conditional distribution (60). We could propose two possible solutions to overcome this problem: running the n GP emulators in parallel at every iteration of the algorithm and speeding up GP evaluations for large datasets through nested predictions (Rullière et al., 2017).

Another tough question concerns the choice of the prior distribution of σ^2 . If an inverse-gamma prior is put on such a scale parameter, as we did in the paper, then its significant prior mass near 0 does not vanish in the posterior distribution (Gelman, 2006). This can thus lead to a Bayesian procedure that is not as much as data-dominated as we want, especially in a small data context.

Lastly, as the posterior samples generated by the GP-based Gibbs algorithm are highly correlated, other proposal densities for the MH algorithm could be tested. In this way, we may

improve the mixing of the Markov chain and therefore the precision of both point estimates and fluctuation intervals.

7. Acknowledgements

The authors would like to thank you the URANIE team for his guidance in using the software as well as a careful reading of the paper. This work has been funded by the tripartite project devoted to Uncertainty Quantification, consisting of French Alternative Energies and Atomic Energy Commission (CEA), Electricity of France (EDF) and Framatome (FRA).

Appendix A. The GP emulator

This appendix provides the mathematical forms of both predictive mean and variance of the posterior GP constructed at $\mathbf{x}_i^f \in \mathbf{X}^f$ with respect to the M learning simulations $Y_{\mathbf{x}_i^f}(\mathbf{D}_M)$. Let us denote the correlation matrix of these simulations by:

$$C_{\mathbf{x}_i^f}(\mathbf{D}_M) = \left[C_{\mathbf{x}_i^f}(\lambda_i, \lambda_j) \right]_{1 \leq i, j \leq M} \in \mathcal{M}_{M, M}(\mathbb{R}) \quad (\text{A.1})$$

Let λ any input value of \mathcal{L} . Then, the vector of the correlations between $Y_{\mathbf{x}_i^f}(\lambda)$ and every component of $Y_{\mathbf{x}_i^f}(\mathbf{D}_M)$ is equal to

$$C_{\mathbf{x}_i^f}(\lambda, \mathbf{D}_M) = \left(C_{\mathbf{x}_i^f}(\lambda, \lambda_1), \dots, C_{\mathbf{x}_i^f}(\lambda, \lambda_M) \right)^T \in \mathbb{R}^M \quad (\text{A.2})$$

The predictive mean at λ is written as the conditional mean of the GP emulator with respect to $Y_{\mathbf{x}_i^f}(\mathbf{D}_M)$:

$$\mu_{\mathbf{x}_i^f}^M(\lambda) = m_{\mathbf{x}_i^f}(\lambda) + C_{\mathbf{x}_i^f}(\lambda, \mathbf{D}_M)^T C_{\mathbf{x}_i^f}(\mathbf{D}_M)^{-1} \left(Y_{\mathbf{x}_i^f}(\mathbf{D}_M) - m_{\mathbf{x}_i^f}(\lambda) \right). \quad (\text{A.3})$$

Let us now consider two input locations $\lambda, \lambda' \in \mathcal{L}$. Then, the predictive covariance is given by

$$V_{\mathbf{x}_i^f}^M(\lambda, \lambda') = \sigma_i^2 \left(C_{\mathbf{x}_i^f}(\lambda, \lambda') - C_{\mathbf{x}_i^f}(\lambda, \mathbf{D}_M)^T C_{\mathbf{x}_i^f}(\mathbf{D}_M)^{-1} C_{\mathbf{x}_i^f}(\lambda', \mathbf{D}_M) \right). \quad (\text{A.4})$$

An important property is that the GP emulator can interpolate the learning simulations, meaning that for every location $\lambda_j \in \mathbf{D}_M$ we have for $1 \leq j \leq M$

$$\mu_{\mathbf{x}_i^f}^M(\lambda_j) = Y_{\mathbf{x}_i^f}(\lambda_j) \quad (\text{A.5})$$

and

$$V_{\mathbf{x}_i^f}^M(\lambda_j, \lambda_j) = 0. \quad (\text{A.6})$$

Appendix B. Proof of Theorem 1

PROOF. The likelihood can be written as

$$\pi(b, \sigma^2, \mathbf{A}' | \mathbf{z}'^f, \mathbf{X}^f) \propto \pi(\mathbf{z}'^f | \mathbf{A}', \mathbf{X}^f, b, \sigma^2) \pi(\mathbf{A}' | b, \sigma^2) \pi(b, \sigma^2) \quad (\text{B.1})$$

where

$$\pi(\mathbf{z}'^f | \mathbf{A}', \mathbf{X}^f, b, \sigma^2) = \prod_{i=1}^n \left(\frac{1}{\sqrt{2\pi\sigma_{\epsilon_i}}} \right) \exp -\frac{1}{2} \sum_{i=1}^n \frac{(z_i^f - h^T(\mathbf{x}_i^f)\alpha'_i)^2}{\sigma_{\epsilon_i}^2} \quad (\text{B.2})$$

$$\begin{aligned} \pi(\mathbf{A}' | b, \sigma^2) &= \left(\frac{|\Sigma|^{-1/2}}{(2\pi)^{p/2}} \right)^n \exp -\frac{1}{2} \sum_{i=1}^n (\alpha'_i - b)^T \Sigma^{-1} (\alpha'_i - b) \\ &= \frac{\prod_{j=1}^p (\sigma_j)^{-n}}{(2\pi)^{pn/2}} \exp -\frac{1}{2} \sum_{i=1}^n \sum_{j=1}^p \frac{(\alpha'_{i,j} - b_j)^2}{\sigma_j^2} \end{aligned} \quad (\text{B.3})$$

and

$$\begin{aligned} \pi(b | \sigma^2) &= \prod_{j=1}^p \pi(b_j | \sigma_j^2) \\ &= \frac{1}{(2\pi)^{p/2}} \prod_{j=1}^p \frac{\sqrt{a_j}}{\sigma_j} \times \exp -\frac{1}{2} \sum_{j=1}^p \frac{a_j (b_j - \mu_j)^2}{\sigma_j^2} \end{aligned} \quad (\text{B.4})$$

$$\pi(\sigma^2) = \prod_{j=1}^p \pi(\sigma_j^2) = \prod_{j=1}^p \frac{(\sigma_j)^{2(-\psi_j-1)}}{\Gamma(\psi_j)^p} \times \exp \sum_{j=1}^p -\frac{\gamma_j}{\sigma_j^2} \quad (\text{B.5})$$

By gathering together Equations (B.3), (B.4) et (B.5) where σ^2 occurs, we have

$$\begin{aligned} \pi(\sigma^2 | b, \mathbf{A}', \mathbf{X}^f, \mathbf{z}'^f) &\propto \prod_{j=1}^p (\sigma_j)^{-(n+1+2(\psi_j+1))} \times \\ &\exp -\sum_{j=1}^p \left[\frac{\sum_{i=1}^n (\alpha'_{i,j} - b_j)^2}{2\sigma_j^2} + \frac{a_j (b_j - \mu_j)^2}{2\sigma_j^2} + \frac{\gamma_j}{\sigma_j^2} \right] \end{aligned} \quad (\text{B.6})$$

We can recognize the probability density of p independent Gaussian-inverse gamma distributions with parameters

$$\psi_j + \frac{n}{2} + \frac{1}{2} \quad (\text{B.7})$$

and

$$\frac{1}{2} \sum_{i=1}^n (\alpha'_{i,j} - b_j)^2 + \frac{a_j}{2} (b_j - \mu_j)^2 + \gamma_j, \quad (\text{B.8})$$

which completes the proof of (32). Now, by gathering together Equations (B.3) et (B.4) containing b , we have

$$\pi(b|\sigma^2, \mathbf{A}', \mathbf{X}^f, \mathbf{z}'^f) \propto \exp - \sum_{j=1}^p \frac{\sum_{i=1}^n (\alpha'_{i,j} - b_j)^2}{2\sigma_j^2} + \frac{a_j(b_j - \mu_j)^2}{2\sigma_j^2} \quad (\text{B.9})$$

$$\propto \exp - \sum_{j=1}^p \frac{\sum_{i=1}^n \alpha'_{i,j}{}^2 - 2b_j \sum_{i=1}^n \alpha'_{i,j} + nb_j^2 + a_j b_j^2 - 2a_j b_j \mu_j + a_j \mu_j^2}{2\sigma_j^2} \quad (\text{B.10})$$

$$\propto \exp - \sum_{j=1}^p \frac{(a_j + n)}{2\sigma_j^2} \left[b_j^2 - \frac{2b_j(n\bar{\alpha}'_j + a_j \mu_j)}{a_j + n} + \frac{\sum_{i=1}^n \alpha'_{i,j}{}^2 + a_j \mu_j^2}{a_j + n} \right] \quad (\text{B.11})$$

$$\propto \exp - \sum_{j=1}^p \frac{(a_j + n)}{2\sigma_j^2} \left[b_j - \frac{n\bar{\alpha}'_j + a_j \mu_j}{a_j + n} \right]^2 \quad (\text{B.12})$$

which proves Equation (31). Lastly, proof of (33) is based on combining Equation (B.2) with Equation (B.3)

$$\pi(\mathbf{A}'|b, \sigma^2, \mathbf{z}'^f, \mathbf{X}^f) \propto \exp - \frac{1}{2} \sum_{i=1}^n \frac{(z'_i{}^f - h^T(\mathbf{x}_i^f) \alpha'_i)^2}{\sigma_{\epsilon_i}^2} + (\alpha'_i - b)^T \Sigma^{-1} (\alpha'_i - b) \quad (\text{B.13})$$

Equation (B.13) is rewritten as

$$\pi(\mathbf{A}'|b, \sigma^2, \mathbf{z}'^f, \mathbf{X}^f) \propto \exp \sum_{i=1}^n \left(-\frac{1}{2} \alpha_i{}^T \left[\frac{h(\mathbf{x}_i^f) h^T(\mathbf{x}_i^f)}{\sigma_{\epsilon_i}^2} + \Sigma^{-1} \right] \alpha_i + \left[\frac{h(\mathbf{x}_i^f) z'_i{}^f}{\sigma_{\epsilon_i}^2} + \Sigma^{-1} b \right]^T \alpha_i \right) \quad (\text{B.14})$$

Furthermore, if for any $\nu \in \mathbb{R}^n$ and any $B \in \mathbb{R}^{n \times n}$ positive definite matrix

$$f(w) \propto \exp - \frac{1}{2} w^T B^{-1} w + \nu^T w \quad (\text{B.15})$$

then $W \sim \mathcal{N}(B\nu, B)$. Proof of (33) is done in applying this lemma to (B.14).

Appendix C. Proof of Theorem 3

PROOF. By applying Bayes formula, the ratio

$$\frac{\pi(\alpha_i(\text{new})|m(s), \sigma^2(s), z_i^f, \mathbf{x}_i^f) \times \pi_{prop}(\alpha_i(s)|m(s), \sigma^2(s), \alpha_i(\text{new}))}{\pi(\alpha_i(s)|m(s), \sigma^2(s), z_i^f, \mathbf{x}_i^f) \times \pi_{prop}(\alpha_i(\text{new})|m(s), \sigma^2(s), \alpha_i(s))} \quad (\text{C.1})$$

is equal to

$$\frac{\pi(z_i^f|m(s), \sigma^2(s), \alpha_i(\text{new}), \mathbf{x}_i^f) \times \pi(\alpha_i(\text{new})|m(s), \sigma^2(s)) \times \pi_{prop}(\alpha_i(s)|m(s), \sigma^2(s), \alpha_i(\text{new}))}{\pi(z_i^f|m(s), \sigma^2(s), \alpha_i(s), \mathbf{x}_i^f) \times \pi(\alpha_i(s)|m(s), \sigma^2(s)) \times \pi_{prop}(\alpha_i(\text{new})|m(s), \sigma^2(s), \alpha_i(s))} \quad (\text{C.2})$$

Then, as $\pi_{prop}(\cdot)$ is chosen as being independent of the current sample $\alpha_i(\cdot)$, then Equation (C.2) is equal to

$$\frac{\pi(z_i^f|m(s), \sigma^2(s), \alpha_i(\text{new}), \mathbf{x}_i^f)}{\pi(z_i^f|m(s), \sigma^2(s), \alpha_i(s), \mathbf{x}_i^f)}. \quad (\text{C.3})$$

Appendix D. Proof of Theorem 4

PROOF. Let

$$Y(\mathbf{D}_M) = \cup_{i=1}^n Y_{\mathbf{x}_i^f}(\mathbf{D}_M) \quad (\text{D.1})$$

be the whole set of simulations for fitting the n GP emulators (one per input site $\mathbf{x}_i^f \in \mathbf{X}^f$) and let $\theta = \cup_{i=1}^n \{\theta_i\}$ be the whole parameters of the GPs with $\theta_i = (\beta_i, \sigma_i^2, l_i)^T$. By following a full Bayes approach, θ is estimated jointly with (m, σ^2) and the posterior distribution of (m, σ^2, θ) is not only conditional on \mathbf{z}^f but also on $Y(\mathbf{D}_M)$. Hence,

$$\pi(m, \sigma^2, \theta, \mathbf{A} | \mathbf{z}^f, \mathbf{X}^f, Y(\mathbf{D}_M)) \propto \mathcal{L}(\mathbf{z}^f, Y(\mathbf{D}_M) | m, \sigma^2, \theta, \mathbf{A}, \mathbf{X}^f) \pi(\mathbf{A} | m, \sigma^2, \theta) \pi(m, \sigma^2, \theta). \quad (\text{D.2})$$

where

$$\mathcal{L}(\mathbf{z}^f, Y(\mathbf{D}_M) | m, \sigma^2, \theta, \mathbf{A}, \mathbf{X}^f) = \prod_{i=1}^n \mathcal{L}_i(z_i^f, Y_{\mathbf{x}_i^f}(\mathbf{D}_M) | m, \sigma^2, \theta_i, \alpha_i, \mathbf{x}_i^f) \quad (\text{D.3})$$

Every one dimensional likelihood $\mathcal{L}_i(z_i^f, Y_{\mathbf{x}_i^f}(\mathbf{D}_M) | m, \sigma^2, \theta_i, \alpha_i)$ is a Gaussian density with a mean equal to

$$(m_{\mathbf{x}_i^f, \beta_i}(\exp \alpha_i), m_{\mathbf{x}_i^f, \beta_i}(\mathbf{D}_M))^T \in \mathbb{R}^{M+1} \quad (\text{D.4})$$

and a covariance matrix equal to

$$\sigma_i^2 \begin{pmatrix} C_{\mathbf{x}_i^f, l_i}(\exp \alpha_i, \exp \alpha_i) + \frac{\sigma_{\epsilon_i}^2}{\sigma_i^2} & C_{\mathbf{x}_i^f, l_i}(\exp \alpha_i, \mathbf{D}_M) \\ C_{\mathbf{x}_i^f, l_i}(\exp \alpha_i, \mathbf{D}_M)^T & C_{\mathbf{x}_i^f, l_i}(\mathbf{D}_M). \end{pmatrix} \in \mathcal{M}_{M+1, M+1}(\mathbb{R}) \quad (\text{D.5})$$

Such a full-Bayes approach requires specifying a prior distribution on θ , which is not always straightforward, in particular for the correlation lengths (Paulo, 2005). Furthermore, we can see that the physical experiments \mathbf{z}^f impact the estimation of θ , whereas we would like that only the learning simulations are used for it. Both of these remarks conduct us to turn to another approach. Equation (60) is actually derived from applying *a modular approach* (Liu et al., 2009) similar to that being carried out in other works dealing with GP-based inverse UQ (Kennedy and O'Hagan, 2001; Bayarri et al., 2007; Fu et al., 2015). This technique neglects the impact of the physical experiments \mathbf{z}^f on the estimation of θ . A point estimate $\hat{\theta}$ is actually estimated only with respect to $Y(\mathbf{D}_M)$ (see Appendix E), then puts into the conditionnal distribution \mathcal{L}^{Cond} of \mathbf{z}^f conditional on $m, \sigma^2, Y(\mathbf{D}_M)$ and \mathbf{A} :

$$\mathcal{L}^{Cond}(\mathbf{z}^f | Y(\mathbf{D}_M), \mathbf{A}, \mathbf{X}^f, m, \sigma^2, \hat{\theta}) = \prod_{i=1}^n \mathcal{L}_i^{Cond}(z_i^f | Y_{\mathbf{x}_i^f}(\mathbf{D}_M), \alpha_i, m, \sigma^2, \hat{\theta}_i) \quad (\text{D.6})$$

where every $\mathcal{L}_i^{Cond}(\cdot | \cdot)$ is a one dimensional Gaussian density with mean equal to

$$\mu_{\mathbf{x}_i^f, \hat{\beta}_i, \hat{l}_i}^M(\exp \alpha_i) \quad (\text{D.7})$$

and variance equal to

$$V_{\mathbf{x}_i^f, \hat{l}_i, \hat{\sigma}_i^2}^M(\exp \alpha_i, \exp \alpha_i) + \sigma_{\epsilon_i}^2 \quad (\text{D.8})$$

with $\mu^M(\cdot)$ and $V^M(\cdot)$ being respectively the conditional mean and variance of the i th GP emulator evaluated at $\hat{\theta}$. Finally, Equation (60) is obtained as the full conditional posterior distribution of \mathbf{A} by replacing $\mathcal{L}(\mathbf{z}^f, Y(\mathbf{D}_M) | \mathbf{A}, \mathbf{X}^f, m, \sigma^2, \theta)$ by $\mathcal{L}^{Cond}(\mathbf{z}^f | Y(\mathbf{D}_M), \mathbf{A}, \mathbf{X}^f, m, \sigma^2, \hat{\theta})$ in Equation (D.2).

Appendix E. Estimation of the hyperparameters

This is done as part of the modular approach explained in Appendix D. The marginal density of $Y(\mathbf{D}_M)$ with respect to θ is written as:

$$\mathcal{L}(Y(\mathbf{D}_M)|\theta) = \prod_{i=1}^n \mathcal{L}_i(Y_{\mathbf{x}_i^f}(\mathbf{D}_M)|\theta) \quad (\text{E.1})$$

where every $\mathcal{L}_i(Y_{\mathbf{x}_i^f}(\mathbf{D}_M)|\theta)$ is a Gaussian density with mean equal to

$$m_{\mathbf{x}_i^f, \beta_i}(\mathbf{D}_M) \quad (\text{E.2})$$

and covariance matrix equal to

$$\sigma_i^2 C_{\mathbf{x}_i^f, l_i}(\mathbf{D}_M). \quad (\text{E.3})$$

We could then compute a Maximum Likelihood (ML) estimate $\hat{\theta} = (\hat{\theta}_1, \dots, \hat{\theta}_n)$ such that

$$\hat{\theta}_i = (\hat{\beta}_i, \hat{\sigma}_i, \hat{l}_i) = \underset{\theta_i}{\operatorname{argmax}} \mathcal{L}_i(Y_{\mathbf{x}_i^f}(\mathbf{D}_M)|\theta_i). \quad (\text{E.4})$$

References

- A. P. Dempster, N. M. L., Rubin, D. B., 1977. Maximum likelihood from incomplete data via the EM algorithm. *Journal of the Royal Statistical Society Series B (Methodological)* 39.
- AIAA, 1998. Guide for the Verification and Validation of Computational Fluid Dynamics simulations. American Institute of Aeronautics and Astronautics.
- ASME, 2009. Standard for Verification and Validation in Computational Fluid Dynamics and Heat Transfer. American Society of Mechanical Engineers.
- Baccou, J., Bestion, B., Damblin, G., Fillion, P., Fouet, F., Freixa, F., ..., 2018. SAPIUM: A Systematic Approach for Input Uncertainty Quantification. In: Best Estimate Plus Uncertainty International Conference, Lucca, Italy.
- Bayarri, M. J., Berger, J. O., Sacks, P. R., Cafeo, J. A., Cavendish, J., Lin, C.-H., Tu, J., 2007. A framework for validation of computer models. *Technometrics* 49, 138–154.
- Belsley, D., Kuh, E., Welsch, R., 1980. "The condition number". in regression diagnostics: Identifying influential data and sources of collinearity. New York: John Wiley and Sons.
- Blanchard, J., Damblin, G., Martinez, J., Arnaud, G., Gaudier, F., Mar. 2018. The Uranie platform: an Open-source software for optimisation, meta-modelling and uncertainty analysis. ArXiv e-prints.
- Boyack, B., Catton, I., Duffrey, R., Griffith, P., Katsma, K., Lellouche, G., Levy, S., U.S., R., Wilson, G., Wulff, W., Zuber, N., 1990. An overview of the code scaling, applicability and uncertainty evaluation methodology. *Journal of Nuclear Engineering and Design* 119.
- Brooks, S., Gelman, A., 1998. General Methods for Monitoring Convergence of Iterative Simulations. *Journal of Computational and Graphical Statistics* 7, 434–455.

- Celeux, G., Grimaud, A., Lefèbvre, Y., de Rocquigny, E., 04 2010. Identifying intrinsic variability in multivariate systems through linearized inverse methods. *Inverse Problems in Science and Engineering* 18.
- Chib, S., Greenberg, E., 1995. Understanding the Metropolis-Hastings algorithm. *The American Statistician* 49(4), 327–335.
- Cowles, M., Carlin, B., 1996. Markov chain monte carlo convergence diagnostics: A comparative review. *Journal of the American Statistical Association* 91 (434).
- Csni, N., 2016. PREMIUM, A benchmark on the quantification of the uncertainty of the physical models in the system thermal-hydraulic codes: methodologies and data review. Tech. rep., csni-r2016-9.pdf.
- Currin, C., Mitchell, T., Morris, M., Ylvisaker, D., 1991. Bayesian prediction of deterministic functions, with applications to the design and analysis of computer experiments. *Journal of the Statistical Association* 86 (416), 953–963.
- Damblin, G., Barbillon, P., Keller, M., Pasanisi, A.; Parent, E., 01 2018. Adaptive numerical designs for the calibration of computer codes. *SIAM/ASA Journal on Uncertainty Quantification* 6.
- D’Auria, F., Carmago, C., Mazzantini, O., 2012. The Best Estimate Plus Uncertainty (BEPU) approach in licensing of current nuclear reactors. *Nuclear Engineering and Design*.
- De Crécy, A., Bazin, P., 2001. Determination of the uncertainties of the constitutive relationship of the CATHARE 2 code. *M&C* 2001.
- De Crécy, A., Bazin, P., Glaeser, H., Skorek, T., Joucica, J., Probst, P., Fujioka, K., Chung, B., Oh, D., Kyncl, M., Pernica, R., Macek, J., Meca, R., Macian, R., D’Auria, F., Petruzzi, A., Batet, L., Perez, M., Reventos, F., 2008. Uncertainty and sensitivity analysis of the loft l2-5 test: Results of the BEMUSE programme. *Nuclear Engineering and Design* 238 (12), 3561–3578.
- Diebolt, J., Robert, C., 1994. Estimation of finite mixture distributions through bayesian sampling. *Journal of the Royal Statistical Society Series B (Methodological)* 56.
- Freixa, J., De Alfonso, E., Reventos, F., 2016. Testing methodologies for quantifying physical models uncertainties. a comparative exercise using circe and iprem (fftbm). *Nuclear Engineering and Design* 305, 653–665.
- Fu, S., Celeux, G., Bousquet, N., Couplet, M., 2015. Bayesian inference for inverse problems occuring in uncertainty analysis. *International Journal for Uncertainty Quantification* 5 (1), 73–98.
- Gaillard, P., Bestion, D., Dor, I., Germain, P., Moutin, F., 2015. The CATHARE code condensation modelling confronted to the TOPFLOW-PTS steady state experiments. In: *Nureth-16, International Topical Meeting on Nuclear Reactor Thermal Hydraulics*, Chicago, IL.
- Gelfand, A., Smith, A. F., 1990. Sampling based approaches to calculating marginal densities. *Journal of the American Statistical Association* 85, 398–409.

- Gelman, A., 2006. Prior distributions for variance parameters in hierarchical models. *Bayesian Analysis* 1, 1–19.
- Geman, S., Geman, D., 1984. Stochastic relaxation, Gibbs distributions and the Bayesian restoration of image. *IEEE Trans. Pattern Anal. Mach. Intell.* 6, 721–741.
- Geweke, J., 1992. Evaluating the accuracy of sampling-based approaches to the calculation of posterior moments. In: *IN BAYESIAN STATISTICS*. University Press, pp. 169–193.
- Ghosh, J., Delampady, M., Samanta, T., 2007. *An Introduction to Bayesian Analysis: Theory and Methods*. Springer Texts in Statistics. Springer New York.
- Glaeser, H., 2008. GRS method for uncertainty and sensitivity evaluation of code results and applications. *Science and Technology of Nuclear Installations* 2008.
- Janicot, A., Bestion, D., 1993. Condensation modelling for ECC injection. *Nuclear Engineering and Design* 145 (1–2), 37–45.
- Kennedy, M., O’Hagan, A., 2001. Bayesian calibration of computer models. *Journal of the Royal Statistical Society, Series B, Methodological* 63, 425–464.
- Liu, F., Bayarri, M., Berger, J., 2009. Modularization in bayesian analysis, with emphasis on analysis of computer models. *Bayesian Analysis* 4 (1), 119–150.
- Metropolis, N., Rosenbluth, A., Rosenbluth, M., Teller, A. Hand Teller, E., 1953. Equations of state calculations by fast computing machines. *J. Chem. Phys.* 21, 1087–1091.
- Müller, P., 1991. *A Generic Approach to Posterior Integration and Gibbs Sampling*. Tech. rep., Purdue University.
- Murphy, K., 2007. *Conjugate bayesian analysis of the gaussian distribution*. Tech. rep.
- Nouy, E., de Crécy, A., 2017. Quantification of the uncertainty of physical models integrated into system thermohydraulic codes. *Nuclear Engineering and Design* 321, 278 – 287, multi-scale multi-physics analysis of reactor transients in the NURES SAFE project.
- Paulo, R., April 2005. Default priors for gaussian processes. *The Annals of Statistics* 33 (2), 556–582.
- Plummer, M., Best, N., Cowles, L., Vines, K., 2006. Coda: Convergence diagnosis and output analysis for mcmc. *R News* 6 (1), 7–11.
URL <https://journal.r-project.org/archive/>
- Robert, C., Casella, G., 1998. *Monte Carlo Statistical Methods*. Springer-Verlag.
- Roberts, G. O., Gelman, A., Gilks, W. R., 2 1997. Weak convergence and optimal scaling of random walk metropolis algorithms. *The Annals of Applied Probability* 7.
- Rullière, D., Durrande, N., Bachoc, F., Chevalier, C., 7 2017. Nested Kriging predictions for datasets with a large number of observations. *Statistics and Computing*.
- Sacks, J., W.J., W., Mitchell, T., Wynn, H., 1989. Design and analysis of computer experiments. *Technometrics* 31, 41–47.

- Santner, T., Williams, B., Notz, W., 2003. *The Design and Analysis of Computer Experiments*. Springer-Verlag.
- Spiegelhalter, D. J., Abrams, K. R., Myles, J. P., 2004. *Bayesian Approaches to Clinical Trials and Health-Care Evaluation*, section 5.7.3. Chichester: Wiley.
- Unal, C., Williams, B., Hemez, F., Atamturktur, S., McClure, P., 2011. Improved best estimate plus uncertainty methodology, including advanced validation concepts, to license evolving nuclear reactors. *Nuclear Engineering and Design* 241, 1813–1833.
- Wu, X., Kozlowski, T., Meidani, H., Shirvan, K., 08 2018. Inverse uncertainty quantification using the modular Bayesian approach based on Gaussian Process, Part 2: Application to TRACE. *Nuclear Engineering and Design* 335.